UNIVERSIDAD CARLOS III DE MADRID

ESCUELA POLITÉCNICA SUPERIOR

CONTINUUM MECHANICS AND STRUCTURAL ANALYSIS DEPARTMENT

BACHELOR THESIS

NUMERICAL STUDY OF THE BEHAVIOUR OF WINGS UNDER DIFFERENT FLIGHT CONDITIONS

AEROSPACE ENGINEERING

AUTHOR: Guillermo Martín Sainero

TUTOR: Carlos Santiuste Romero

September, 2017

Abstract

The project consists on the numerical analysis of wings to support all loads during flight phases. The A340 600 wing is taken to perform a numerical aerodynamic analysis to obtain the desired flight loads through 3D Panel Method with XFLR5 tool and then numerical structural analysis to study failure criteria, and maximum vertical displacement of the wing when it is used different materials and different thicknesses at any of the different flight phases, through Finite Element Method using Abaqus/CAE software. After that, it is performed an optimization so that it can be obtained a lighter wing that do not fracture, buckles or cracks. This optimization also allows to reduce costs.

Acknowledgments

First of all, I would like to express my all gratitude to my tutor Prof. Carlos Santiuste Romero for trusting, helping and supporting me to carry out this thesis along these months. I would like also to thanks Prof. Oscar Flores Arias by helping me in a part of the project to continue with my bachelor thesis.

I would like to thank people, from 1993 and 1994 of aerospace engineering, all good moments that I have lived in the university, from the first course until now. All of them has helped me to forget and survive in this kind of hell, because aerospace engineering is dark and full of terrors.

Out of the university, I would like to thank all people that helped me to disconnect from this world. Pablo, Rubén, Lucía, María, Najib, Laura, Huguet, Lorena, Cerisola, Rober, Andrés, Pepo, Patricia, Gualber, Chechu and guys that I probably forget right now, are the main responsible people to enjoy this stage of life. Thanks Gonzalo, to be my confident and being like a brother. Also, I want to mention my two best friends Alvaro and Patryk, that they are still stand and support me for a while, since we were at High School.

Although time has spent very quickly, Mr. Guillermo Martín remembers.

I want to thank Cristina AKA Lilass, all the support that she gave and gives me throughout this time. You have been my moral motivation to end this degree up. Your company made me that bad moments has been converted in happy moments. Never forget it.

I do not want to forget about Toan. I will not be here without you. We met when we were six years old in school camp, we have been in the same High School and we finished the same career in the same university, too much time sharing good moments. I have never met any guy like you, an example of goodness, kindness, hard-working and solidarity. You are an example for all people. I always say to you that you must not never forget who you are and why you are where you are, because being the way you are, you will not have problems along your entire life.

Finally, I would like to end with my whole family. First my elder brother and sister that gave me support from the distance to end this career. And then closer, I want to thank from my deepest part of my heart to my parents. I will not be the person that I am without you. Thanks for your love, support and the opportunity you gave me to achieve something as big as this.

Contents

List of Figures

Chapter 1

Chapter 2

Chapter 3

Chapter 4

List of Tables

Chapter 2

Chapter 3

Chapter 4

Chapter 5

Chapter 6

List of Symbols

a_∞	Free stream speed of sound
C_L	Lift coefficient
C_p	Pressure coefficient
E	Young modulus
E_1	Longitudinal modulus
E_2	Transverse modulus
f	Compressibility correction factor
g	Gravity
G_{12}	In-plane shear modulus
G_{13}	Out-of-plane shear modulus
G_{23}	Out-of-plane shear modulus
L	Lift
M_∞	Free stream Mach number
Pr	Prandtl number
P_∞	Free stream pressure
P_0	Pressure at Sea Level
S	Surface
S_L	Longitudinal shear stress
S_T	Transverse shear stress
T_∞	Free stream temperature
T_0	Temperature at Sea Level
U_{MAX}	Maximum vertical displacement
U_∞	Free stream speed
V_{app}	Approaching speed
V_{CAS}	Calibrated Airspeed
V_{EAS}	Equivalent Airspeed
V_{IAS}	Indicated Airspeed
V_{LOF}	Lift-off speed
V_R	Rotational speed

V_{Stall}	Stall speed
V_{TAS}	True Airspeed
V_{Td}	Touchdown speed
V_0	Initial speed
V_1	Decision speed
V_2	Initial climb speed
W	Weight
X_C	Longitudinal compressive stress
X_T	Longitudinal tensile stress
Y_C	Transverse compressive stress
Y_T	Transverse tensile stress
α	Angle of attack
γ	Climb angle
Λ_{LE}	Swept angle
ν	Poisson's ratio
ρ	Material density
ρ_∞	Free stream density
ρ_0	Density at Sea Level
σ_{VM}	Von Mises stress
σ_y	Yield stress
σ_{11}	Principal stress at 11
σ_{22}	Principal stress at 22
σ_{33}	Principal stress at 33

Chapter 1

Introduction

1.1 Background and Motivation

In aeronautics, wings are one of the most important parts in the aircraft from aerodynamic point of view. Their function is to produce enough lift so that aircraft can perform all phases during the flight. Lift is produced due to a pressure difference when the flow is upstream: high pressure at the lower surface and low pressure at the upper surface of the wing.

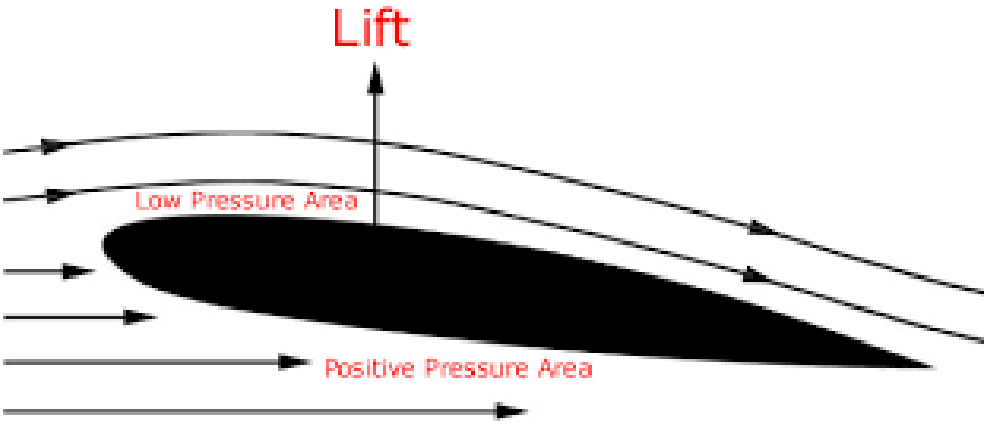

Figure 1.1 - Airfoil generating Lift force [1]

Lift and pressure are completely important in order to perform the structural analysis of the wing, because wing must not fail at any of the different flight phases. Loads applied on the wing are the aerodynamic loads. Since the wing works as a beam, it must stand all the internal forces, i.e. shear, bending and torsion.

A wing is composed of external and internal structural parts that adjusts the loads in each flight phase. It is also made up of high-lift devices, like flaps or slats, that are needed to produce enough lift in flight phases like take-off or landing, so that the aircraft will not stall. Flaps belong to actuators in aircraft systems. There are more actuators, like spoilers to destroy lift and create induced drag, or ailerons for rolling the aircraft.

The external and internal parts of the wing are the following ones:

- Spars: beams that take loads along the wing, from fuselage to wing tip. They take both aerodynamic loads and weight. Inertial loads are very small in comparison son they are neglected. They support the rib attachment and provides stiffness at the whole flight phases.

- Ribs: determine both shape and thickness of the wing and are distributed along the span and perpendicular to spars. This structure is accommodated to the airfoil shape and it is useful for getting the aerodynamic forces.
- Stringers/Stiffeners: Run spanwise and are attached between ribs and skin. They provide to ribs and spars the bending loads and reinforce the skin. They are useful preventing buckling in compression.
- Skin: the external surface of the wing whose function consists on transmitting the aerodynamics forces to internal structures mentioned above.

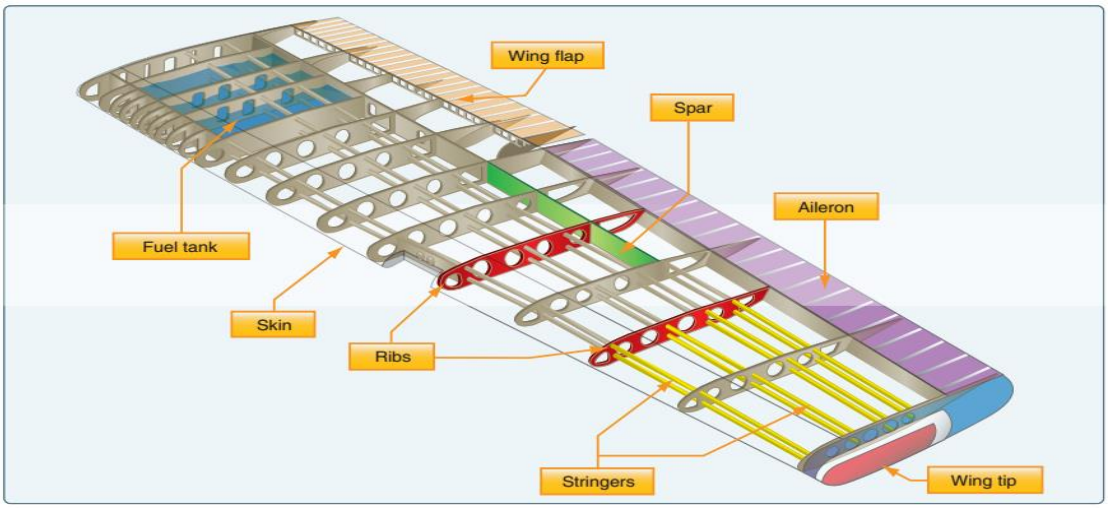

Figure 1.2 - Structural parts of the wing [2]

An aircraft must stand a set of standards and regulations that provides safety and security to passengers during all flight phases, from take-off to landing. These standards and regulations define the different requirements that the aircraft must fulfil in order to safely withstand the different load configurations during the flight, as it is shown in Figure 1.3.

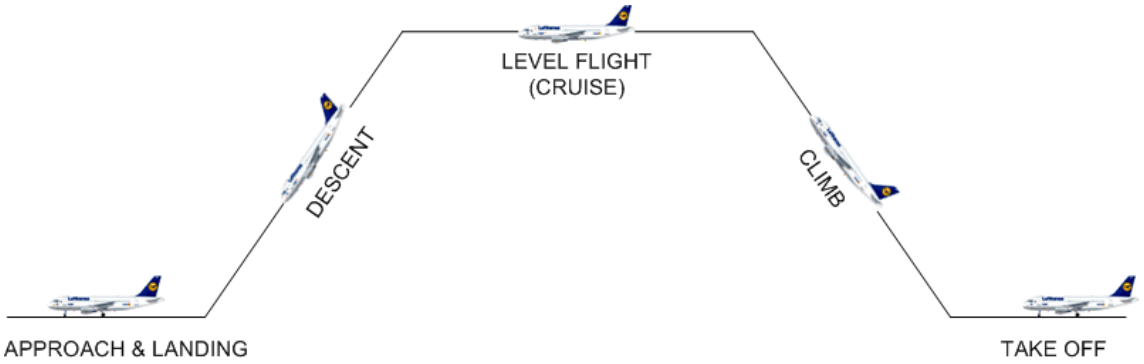

Figure 1.3 - Flight phases of the aircraft [3]

Thus, the wing must support the different load conditions at each flight phase and avoid failure. A brief explanation of the following phases is described below:

- Take off: initial flight phase that goes from zero speed (brakes released from pilot) and accelerates until the aircraft is up to 50 ft from the ground. The flaps are extended in this phase to provide lift to the aircraft and do not lead to stall. This phase is composed of a set phases:
    - Acceleration with all wheels on the ground: the aircraft starts accelerating from $V_0 = 0$ to the minimum speed in take-off V_1.
    - Acceleration with main gear on the ground: aircraft rotates until nose gear is not touching the ground so that $N_{NG} = 0$. The speed in this phase is also known as rotation speed V_R. This phase ends when the main gear is not touching the ground and the speed at the end of this phase is the lift off speed V_{LOF}.
    - Airborne acceleration: the aircraft performs an arc of circumference as a trajectory.
- Steady climb: The aircraft ascends at constant climb angle until reaches 50 ft above the ground to change to climbing phase. The speed in this phase is $V_2 = 1.2V_{stall}$

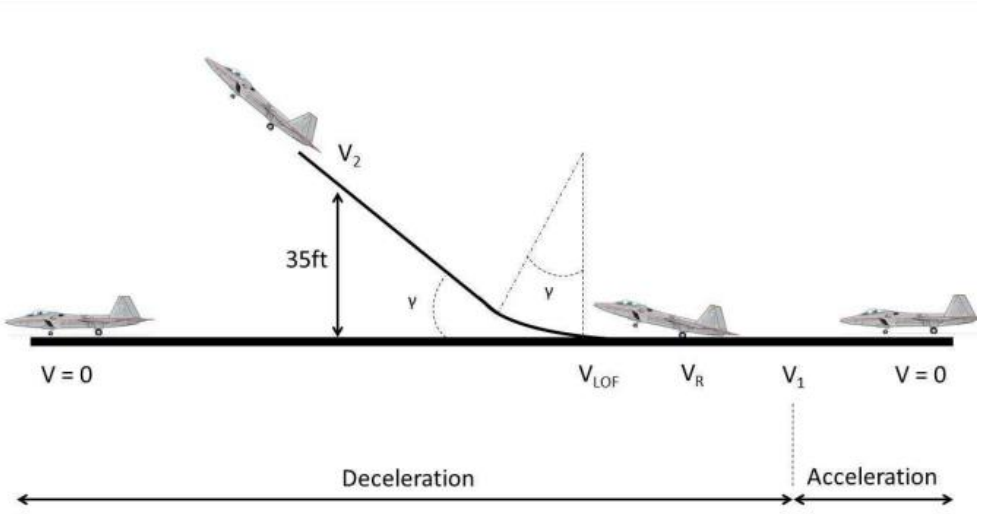

Figure 1.4 - Take-off phases [4]

- Climb: this phase consists on ascending the aircraft at certain cruise altitude at a constant climb angle after taking off. The lift must be higher than weight and this is accomplished by changing the angle of attack or increasing the thrust in engines. This phase ends up when level flight is achieved and the lift force and weight are equal.
- Cruise: In terms of efficiency, this is the most important phase, because most of the time is spending at this one and the fuel consumed is the highest. It consists on heading aircraft at steady flight level. Altitude and speed remain constant, the climb angle is zero, and the sum of whole forces is equal to zero. Therefore, lift equals weight and thrust equals drag.
- Descent: the aircraft decreases altitude. It is an essential phase when approaching to landing. This phase can take place at constant speed and angle of descent.

- Landing: final flight phase that consists on returning the aircraft to the ground. Landing last from 50 ft over the ground until the aircraft stops. The speed is decreased to be low or almost zero, by using brakes and flaps in landing configuration. Landing is divided into three following phases:
    - Final approach: travels a segment at a constant descend angle. To avoid stall, the speed must be $V_{app} \geq 1.3V_{stall}$
    - Landing flare: consists on raising aircraft nose to touch the ground with main landing gear. The speed of this phase is also known as touchdown speed and must be $V_{td} = 1.1V_{stall}$.
    - Ground segment: similar to acceleration with all wheels on the ground, but in this case, is fully reversed, since this phase ends at zero speed, so it is decelerating.

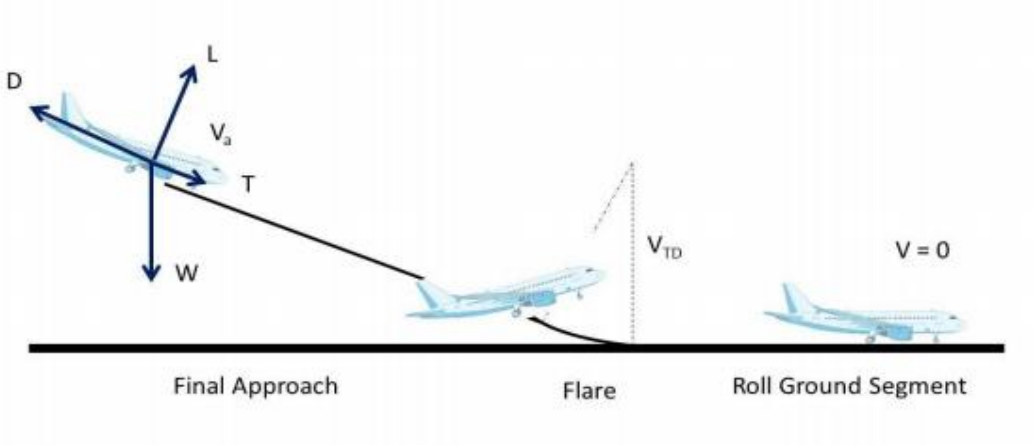

Figure 1.5 - Landing phases [4]

1.2 Objectives of the project

The main objective of this project is the design and optimization of a wing that can support the aerodynamic flight loads in the whole flight. A numerical aerodynamic analysis is used for obtaining the aerodynamic forces and pressures around the wing, by means of 3D panel method. A numerical structural analysis is carried out by means of FEM computation to optimize the wing design. This last analysis is performed without considering the study of buckling, fracture, fatigue. It is just considered failure criteria for different materials.

All the objectives included for the project are represented below:

- Design a wing to perform 3D panel method to obtain aerodynamic forces.
- Understand main aerodynamic differences of each phase when numerical panel method is carried out.

- Understand the importance of each failure criteria to avoid structural failure when numerical analysis through FEM is carried out in each phase performed by the aircraft.
- Optimize to obtain a lighter wing for the aircraft through the use of finite element model.
- Understand the behaviour of carbon fiber material under different load conditions.
- Improve skills of software, like XFLR5 or Abaqus to solve aerodynamic and structural problems.

1.3 Description of the project

This document is divided into 7 Chapters. In this section, the entire composition of all chapters is explained.

- Chapter 1 shows a brief introduction of the project and is separated into three sections. The motivation to explain the problem that is performed in this project, the main objectives of the project to get the desired aims and finally, an exposition of the contents of the project.
- Chapter 2 exposes the state of art of the project, in which relates the current project with past projects. The main specifications of the aircraft, such as dimensions or performances, are part of the content of this chapter. It also covers the theoretical background of 3D Panel Method and XFLR5, which describes the aerodynamic analysis of the wing. Moreover, the theoretical background of Finite Element Method (FEM) and Abaqus/CAE Software are explained to facilitate the structural analysis of the wing. The results of numerical aerodynamic analysis are used as an input to analyse the wing structure by Finite Element Analysis.
- Chapter 3 describes the numerical aerodynamic analysis of the wing to obtain pressure differences around it. This analysis is carried out by using 3D Panel Method using XFLR5 to obtain pressure coefficients distributed around chord and span of the wing in incompressible regime. Bernoulli equation is used to obtain pressure difference depending on the phase the aircraft is performing, so equations of motion are used to obtain lift coefficients and Angles of Attack.
- Chapter 4 presents the numerical structural analysis of the wing. Failure criteria is analysed for different materials by Finite Element Method using Abaqus/CAE. The wing is modelled and meshed to carry out this method, and the results obtained from previous chapter are retrieved and used as an input for the analysis. Moreover, an optimization by changing materials or thicknesses is performed to obtain a lighter wing in order to reproduce a real wing design process.

- Chapter 5 collects all data related to project planning in order to know the estimated hours applied to elaborate all project working phases and how are distributed to follow a right sequence.
- Chapter 6 provides the regulatory and socioeconomic framework and the budget of the project.
- Chapter 7 ends with a summary of the project and conclusions from all ideas argued.

Chapter 2

State of Art

2.1 A340-600 project

A description of the main characteristics and specifications of the A340-600 aircraft is shown in this chapter. This is a previous project in which the reference is taken for elaborating the new wing in this current project.

2.1.1 Characteristics

The Airbus A340 aircraft is a low-wing with four engines developed by Airbus company. Compared with other Airbus aircraft, the A330, A340 200 and A340 300 share the same wide body fuselage and wing design. The A340 500 and A340 600 which were developed later had a larger wing as they were designed for long non-stop flight routes. Coming in four models of varying fuselage length, the A340 was developed for long distance flight at a time when the long distance twin jets of today were yet to make their mark.

Figure 2.1 - A340 600 [5]

The A340 600 was developed to be long range high capacity airliner. Particularly the A340 600HGW (High Gross Weight) model. Other than their longer fuselages, compared to the A340 200 and A340 300, they were also distinguishable by their four-wheeled under fuselage centre wheel bogie. The A340 600 sported the same centre under fuselage bogie but with 4 wheels

instead of 2. This was to support the significantly higher weights that these two aircraft were capable of lifting. [6]

2.1.2 Specifications

This picture below represents the front, top and side view of the A340-600. It can be appreciated the main lengths of the aircraft, i.e. wingspan, fuselage diameter. These measurements are used to accurately define the wing used in the current project.

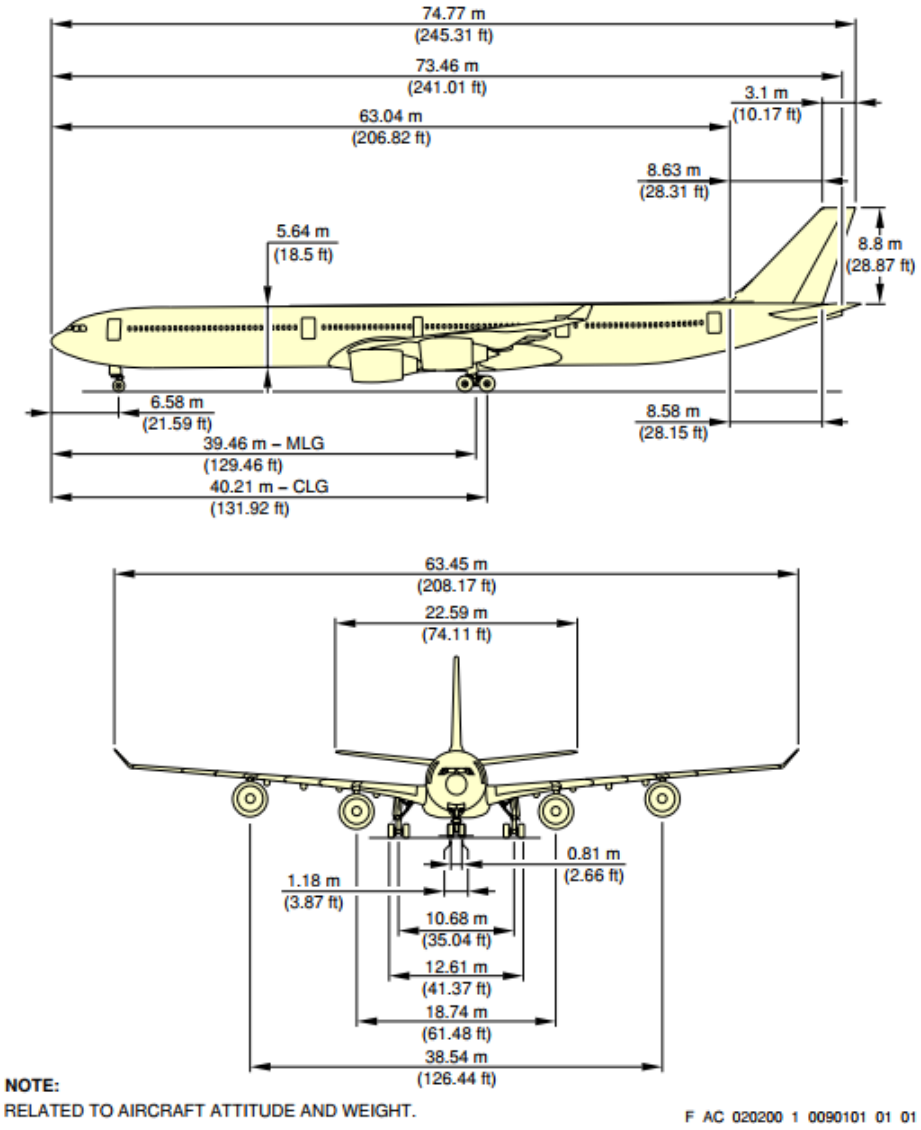

Figure 2.2 - Front and side view of A340 600 with main dimensions [7]

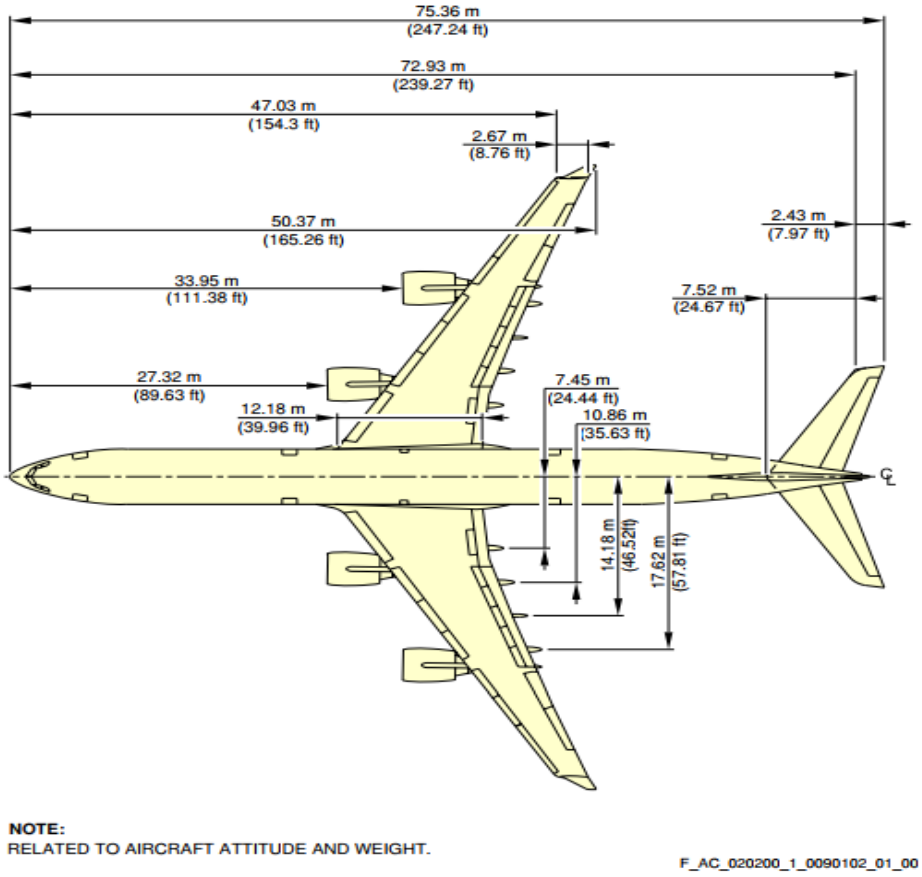

Figure 2.3 - Top view of A340 600 with main dimensions [7]

Moreover, another data retrieved from A340-600 specifications are used to perform the numerical aerodynamic and structural analysis. These specificiations are depicted in Table 2.1:

Specifications	
Wingspan	63.45 m
Root Chord	12.18 m
Tip Chord	2.67 m
Wing Surface	437.3 m^2
Swept Angle	31.1 deg
Fuselage Width	5.64 m
MTOW	368000 kg
MLW	259000 kg
Normal Cruise Mach Number	0.82 @h=36kft
Max Cruise Mach Number	0.86 @h=36kft
Ceiling	12496.8 m
Stall speed	246 km/h
Climb rate	4000 fpm

Table 2.1 - A340 600 specifications [7]

2.2 3D Panel Method

2.2.1 Theoretical Background

3D Panel Method is used in aerodynamics to solve forces and moments acting on an aircraft in flight. Also, solves numerically both thickness and Camber + Angle of Attack problems. It refines LLT and VLM results by a more sophisticated full 3D method, considering wings' thickness. The principle of a 3D Panel Method is to model the perturbation generated by the wing by a sum of doublets and sources distributed over the wing's top and bottom surfaces. The strength of the doublets and sources is calculated to meet the appropriate boundary conditions, which may be of the Dirichlet or Neumann type. In a 3D-Panel calculation, the BC may be either of the Neumann or Dirichlet type. In the latter case the velocity's potential on the panel's inside surface is zero, so that the total potential inside the body is equal to the freestream velocity's potential. Besides, the wing is discretized in panels so that it has constant strength panels. More panels are placed at the LE, so more detailed C_p distribution at LE is obtained. Since it models 3D surface, its approximation of the LE suction peak is better than other numerical methods, i.e. NLSM. This method is the most suitable because it can be taken in a better way the pressure coefficient at both upper and lower surfaces. This analysis is assumed to be:

- Steady flow $(\frac{d}{dt} = 0)$
- Adiabatic $(Pr = 0.7)$
- High Reynolds number $(Re \gg 1)$
- Incompressible flow $(\rho = constant)$
- Inviscid flow
- No gravity

2.2.2 XFLR5

XFLR5 is a software tool in which numerical aerodynamic analysis can be performed. This program gives a graphical user interface for the text-based XFOIL program. XFLR5 can be analysed through Lifting Line Theory or Vortex Lattice method. Besides, it can perform a 3D panel analysis. [7]

In this part, it is presented the different modules that are used for wing and airfoil analysis:

➢ Direct Foil Design Module

This module is used to define the airfoil profiles that are analysed. The process to follow to define it, is:

Introduce the airfoil coordinates. Those coordinates will be dimensionless at the chord and only two methods are valid to introduce the airfoil:

- By means of a .dat file that incorporates all the points for each airfoil.
- By means of an assistance that incorporates a database for some airfoils with characteristic numerology, like NACA.

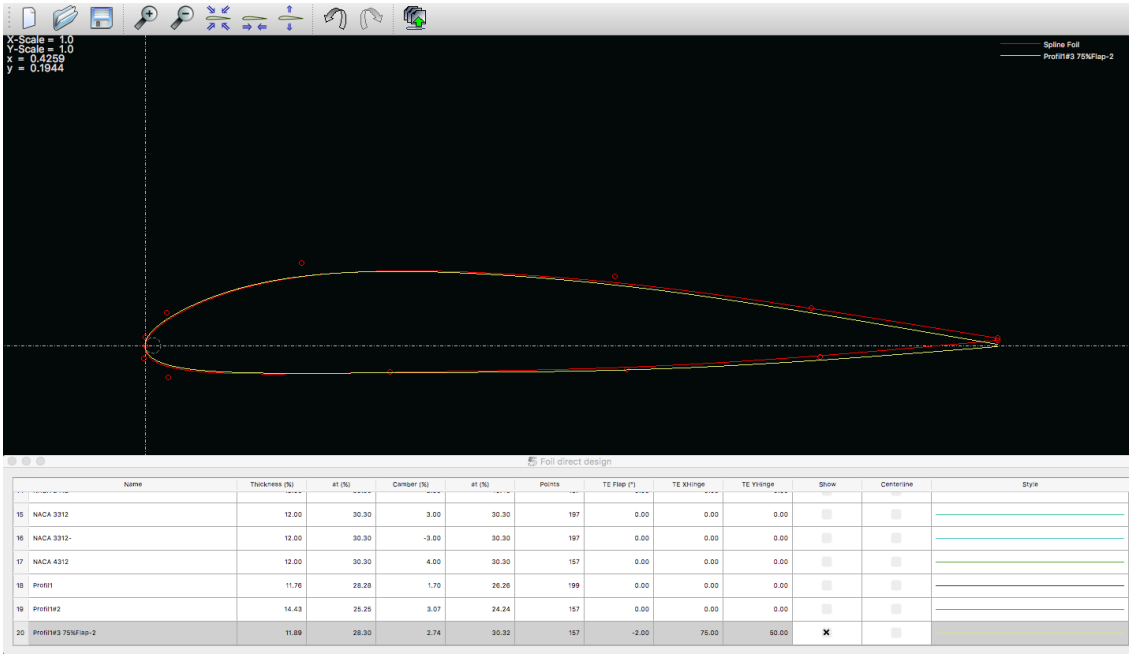

Figure 2.4 – Direct foil design module

➢ XFoil Direct Analysis Module

In this module, it is carried out the analysis over different airfoils defined in previous module. Polars obtained are used to interpret properties and characteristics of the desired airfoil in 2D. These polars, are used in the next module to perform the aerodynamic analysis of complete aerodynamic surfaces.

The analysis can be performed in two ways:

- Manual: From ‘’Analysis’’ the option ‘’Define Analysis’’ at a Reynolds.
- Sequential: ‘’Batch Analysis’’ option to perform the analysis in a range of Reynolds at a fixed increment. This is chosen after selecting a foil and the type of analysis. Finally, it is defined the range of AoA.

This module is discarded in the case that viscosity is neglected in the next module using 3D Panel Method

➢ Wing and Plane Design Module

This section is used to translate the wing geometry to XFLR5 and then performing a wing analysis.

- Translating the wing geometry to XFLR5:

Selecting the option ''Define a New Wing'' from ''Wing-Plane'' Menu is used to introduce the wing in XFLR5. Then an interface appears with a predefined and standard wing that can be modified. In this interface, it can be modified all the characteristics of the wing, i.e. span, chord, swept angle, dihedral, twist. Also, depending on the number of sections, it can be introduced the airfoil/airfoils analysed in the modules described above. It can be introduced the number of panels in X and Y directions.

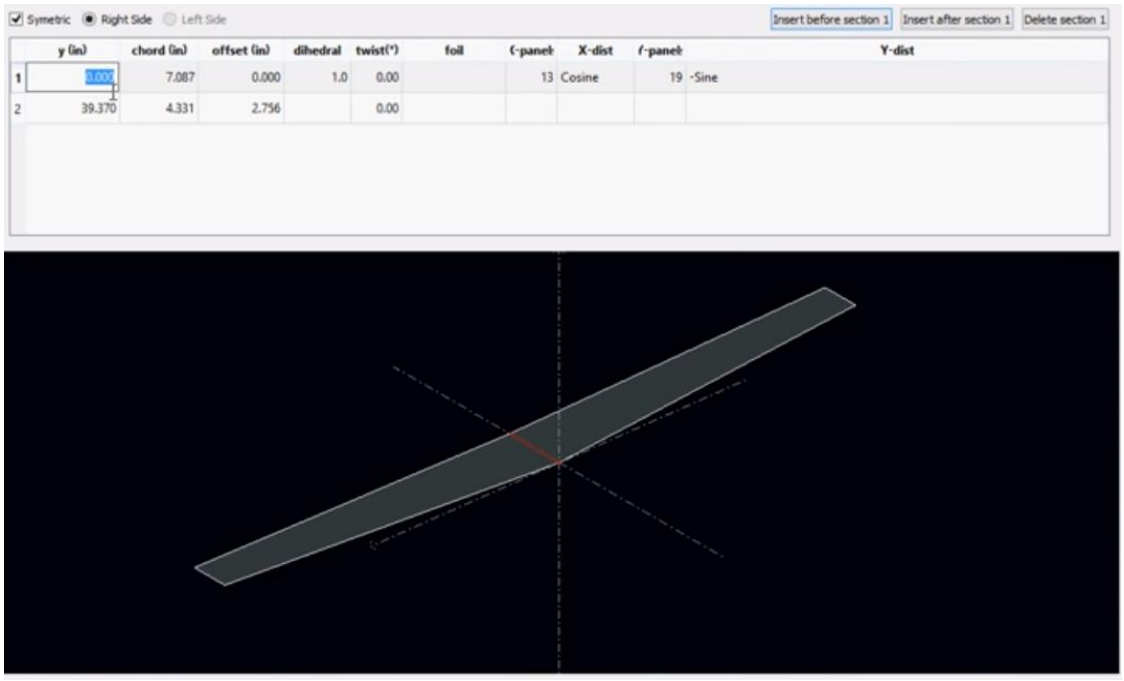

Figure 2.5 – Wing and Plane Design Module

- Wing analysis:

To perform the wing analysis, the first step is ''Define an Analysis'' from ''Polars''. A window is opened to define all the analysis conditions:

- Polar type: it is chosen the desired type of analysis. Type 1 corresponds to constant speed. Type 2 corresponds to constant lift and type 4 corresponds to constant angle of attack.
- Plane and Flight Data: Depending on the analysis chosen, it is introduced the speed, angle of attack that the aircraft will have.
- Aerodynamic Data: Defines density and viscosity conditions.
- Inertia properties: Defines the aircraft mass and the centre of gravity
- Wing analysis methods: The methods that appears are LLT, VLM and 3D.
- Options: ''Viscous'' must be active for the simulation that includes viscous characteristics analysed in 2D
- Ground effect: Defines the ground effect influence.

After defining the AoA sequence, it is clicked on ''Analyze'' button. It is convenient that ''Store OpPoint'' option is active.

2.3 Finite Element Method

2.3.1 Theoretical Background

Finite element method (FEM) is a numerical method applied in structural analysis that solves differential or integral equations and it is used to physical problems, where the governing differential equations are available. The method consists of assuming the piecewise continuous function for the solution and obtaining the parameters of the functions. The objective is to minimize the error in the final result. The method is used to calculate streses, movement of loads, displacements and other physical behaviours. [9]

It is also used to approximate solutions to problems with many complex variables. Integrated FEM is used for design and development of products. FEM generates stiffness and strength visualizations and also is used to optimize weight and costs.

Considering an spatial domain V, it is divided into a number of elements called finite elements.

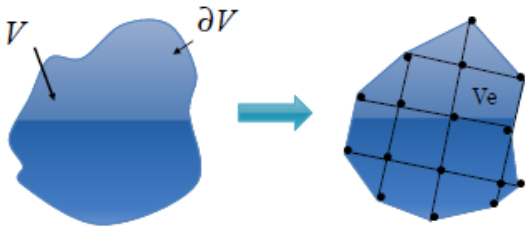

Figure 2.6 – Spatial domain converted into mesh [9]

There are two restrictions that mesh must verify:

- Elements cannot exceed any zone of the domain
- Elements cannot overlap

Each finite element "e" has a specific quantity of nodes m_e, numbered with an index $i (i = 1, \dots, m_e)$.

Finite number of unknowns are obtained from finite element discretization:

- Dividing into elements
- Interpolation functions that are defined at the nodes or nodal points.

Linear combination of interpolation function:

$$\{u^{(e)}\} = [N^{(e)}]\{q^{(e)}\} \tag{2.1}$$

where $q^{(e)}$ contains the N_e displacements of the m_e , and $N^{(e)}$ is the matrix which contains the e-th element interpolation functions (shape functions).

$N^{(e)}(x) = 0$ if x is outside the element e

$$u_i = \sum_{j=1}^{N_e} N_{i,j}^e (x, y, z) q_j^e = u_i^e (x, y, z) \text{ for x inside "e"} \tag{2.2}$$

In the theoretical basis, the formulation of the material properties has three different approaches:

- Direct approach: Related to the direct stiffness method.
- Variational approach: potential energy, complementary energy…
- Weighted residuals approach: No functional is available.

The second approach is used to take the total potential energy of the system.

$$\pi \approx \sum_{e=1}^{E} \pi_e \tag{2.3}$$

$$\pi_e = \int_{V_e} U dv - \int_{V_e} \vec{u} \cdot \overline{f_v} dv - \int_{S_{et}} \vec{u} \cdot \vec{t}\, ds \tag{2.4}$$

where π_e is the total potential energy of an element "e", V_e is the volume of element "e", $\overline{f_v}$ the body Surface and S_{et} is the e-th surface.

From equation (2.4), the first integral of the total potential energy corresponds to the strain energy stored in the element, the second integral is the work potential of the body force, and finally, the third integral defines the work potential of surface forces.

The strain energy stored is defined as a function of the deformation tensor and strain:

$$U = \frac{1}{2}\{D\}^T(\sigma) \tag{2.5}$$

$$U^e = \frac{1}{2}\{D^e\}^T[C]\{D^e\} \tag{2.6}$$

$$\{D^e\} = [L]\{u^e\} = [L][N^e]\{q^e\} = [B]\{q^e\} \tag{2.7}$$

$$\pi = \sum_{e=1}^{E} \pi^e = \sum_{e=1}^{E} (\frac{1}{2}\{q^e\}^T[K^e]\{q^e\} - \{q^e\}^T\{Q^e\}) \tag{2.8}$$

Joining the element properties to get the system of equations → an element connectivity matrix has to be defined. Using the following properties:

$$\{q^e\} = [A^e]\{q\} \tag{2.9}$$

$$\{q^e\}^T = ([A^e]\{q\})^T = \{q\}^T[A^e]^T \tag{2.10}$$

$$\pi = \frac{1}{2}\{q\}^T \sum_{e=1}^{E} ([A^e]^T[K^e][A^e]\{q\} - \{q\}^T \left[\sum_{e1}^{E} ([A^e]^T\{Q^e\})\right] \tag{2.11}$$

$$\pi = \frac{1}{2}\{q\}^T[K]\{q\} - \{q\}^T\{Q\} \tag{2.12}$$

where K is the global stiffness matrix and Q is the global forcing vector, which are known. [9]

2.3.2 Abaqus

Abaqus/CAE is a software used in aerospace industry that creates models and analyse their structural by means of simulations. Abaqus/CAE is splitted into modules, for example, defining the part, material properties, sections, loads and mesh. Displacing through these modules, it is modelled components in which Abaqus/CAE generates an input file that is submitted to the Abaqus/Standard analysis product. The analysis product sends information to Abaqus/CAE to allow to progressing on the job, and generates an output database. Finally, it is used the Visualization module to view and check the results obtained. [10]

It can be divided FEA into three main following steps: [11]

- Pre-processing: In this step, it is defined the model of the physical problem and create an Abaqus input file. The model is created, the materials and sections are defined, the loads are introduced and the model is meshed.
- Processing: The simulation, which normally is run as a background process, is the stage in which Abaqus/Standard or Abaqus/Explicit solves the numerical problem defined in the model and produces an output visual file. Displacements and stresses that are stored in binary files are ready for post-processing.
- Post-Processing: It is generated a result from the output file. Results are evaluated once the simulation has been completed and the displacements or stresses are computed, and can be checked in visualization module. This module, has a lot of options when results are displayed.

In order to carry out these processes, a set of modules are in the software to separate each steps. [10]

➢ PART MODULE

The Part module allows to do the following:

- Create deformable, discrete rigid, analytical rigid, or Eulerian parts. The part tools also allow you to edit and manipulate the existing parts defined in the current model.
- Create the features—solids, shells, wires, cuts, and rounds—that define the geometry of the parts.
- Use the Feature Manipulation toolset to edit, delete, suppress, resume, and regenerate a part's features.
- Assign the reference point to a rigid part.
- Use the Sketcher to create, edit, and manage the two-dimensional sketches that form the profile of a part's features. These profiles can be extruded, revolved, or swept to create part geometry; or they can be used directly to form a planar or axisymmetric part.
- Use the Set toolset, the Partition toolset, and the Datum toolset. These toolsets operate on the part in the current viewport and allow you to create sets, partitions, and datum geometry, respectively.

➢ PROPERTY MODULE

It is used to perform the following tasks:

- Define materials.
- Define beam section profiles.
- Define sections.
- Assign sections, orientations, normals, and tangents to parts.
- Define composite layups.
- Define a skin reinforcement.
- Define inertia (point mass, rotary inertia, and heat capacitance) on a part.
- Define material calibrations

➢ ASSEMBLY MODULE

It is used to create and modify the assembly. A model contains one main assembly, which is composed of instances of parts from the model as well as instances of other models.

➢ STEP MODULE

It is used to perform the following tasks:

- Create analysis steps.
- Specify output requests.
- Specify analysis controls.

➢ LOAD MODULE

You use the Load module to define and manage the following prescribed conditions:

- Loads
- Boundary conditions
- Predefined fields
- Load cases

- **MESH MODULE**

The Mesh module contains tools that allow you to generate meshes on parts and assemblies created within Abaqus/CAE. In addition, the Mesh module contains functions that verify an existing mesh.

- **JOB MODULE**

It is used to create and manage analysis jobs and to view a basic plot of the analysis results. You can also use the Job module to create and manage adaptivity analyses and co-executions.

- **VISUALIZATION MODULE**

It is used to view your model and the results of your analysis.

Chapter 3

Numerical Aerodynamic Analysis

In this chapter, it is explained the use of 3D Panel Method for the numerical aerodynamic analysis of the desired wing. This method is useful for obtaining the pressure distribution around each airfoil section and along the wing so that it can be used for the structural analysis. Therefore, the design of both airfoil and wing are modelled for carrying it out.

3.1 Geometry

3.1.1 Airfoil Section

Firstly, it must be defined the section of the wing through the direct foil design module in XFLR5. The airfoil can be defined either with dat files or retrieving it from the database, like NACA foils.

The desired airfoil must generate high lift and maximum lift coefficient. Thus, it must be divided into symmetric and asymmetric.

- Symmetric: same upper (extrados) and lower (intrados) surfaces and no camberline, since the chordline goes from Leading Edge to Trailing Edge. This type of airfoils, are low-cost and easy-build but produce less lift, having no desirable stall characteristics.
- Asymmetric: different upper and lower surfaces so in this case there is camberline. These airfoils generate higher lift w.r.t symmetric ones. The most important inconvenience of asymmetric airfoils is the pitching moment generated.

Therefore, it must be selected an asymmetric section due to it is not taken into account the longitudinal stability in this project. The chosen airfoil is NACA6415 and it is represented below with its respective points at extrados and intrados:

EXTRADOS		**INTRADOS**	
x/c	**y/c**	**x/c**	y/c
1.000	0.000	0.000	0.000
0.800	0.067	0.100	-0.032
0.600	0.111	0.200	-0.027
0.400	0.133	0.400	-0.012
0.200	0.120	0.600	-0.002
0.100	0.086	0.800	0.000
0.000	0.000	1.000	0.000

Table 3.1 - NACA6415 Foil Coordinates [12]

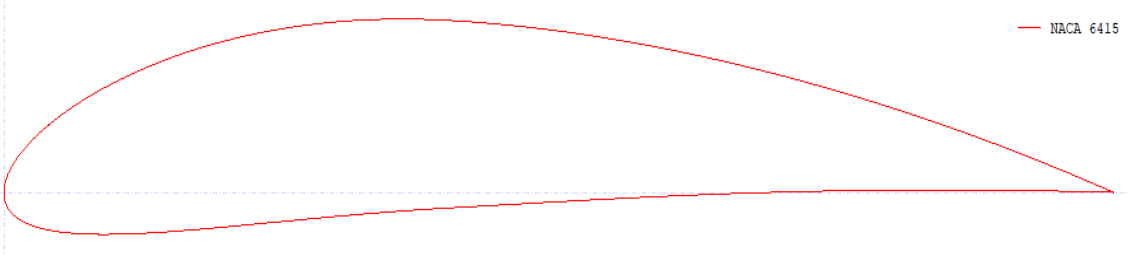

Figure 3.1 - NACA 6415 Foil using XFLR5

3.1.2 Wing Section

The specifications of the geometry of the wing are data retrieved from A340-600 and it is designed for the aerodynamic analysis.

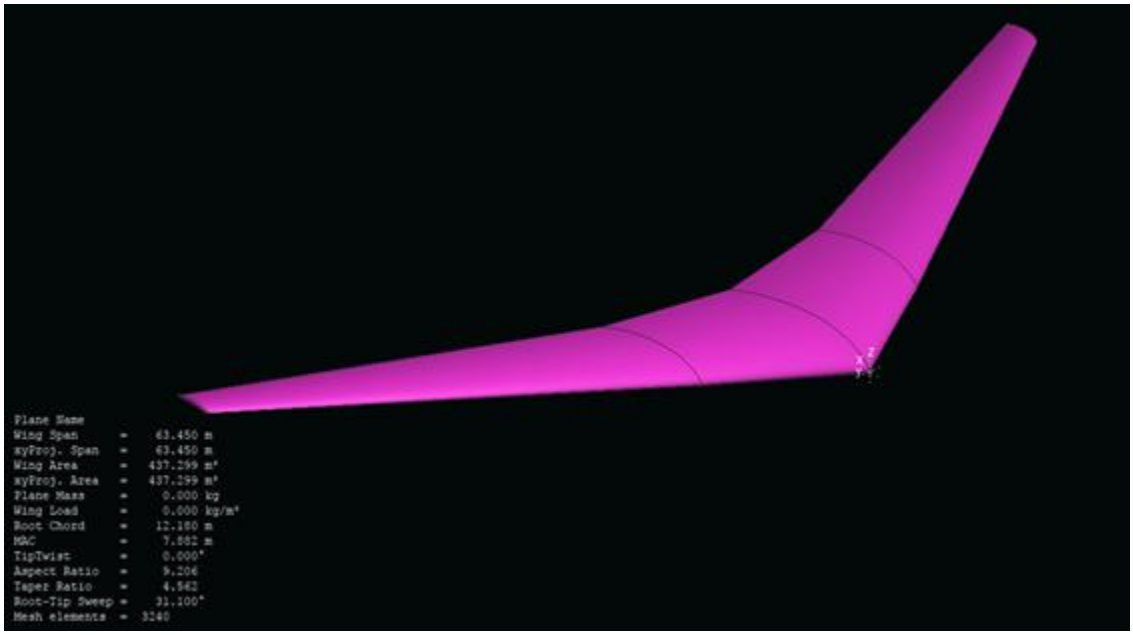

Figure 3.2 - A340 600 Wing Design

The real wing has winglets at the wingtip, but they are deleted in this new model, so it can be modelled in an easiest way. Also, it is assumed to have no twist and no dihedral.

After designing both airfoil and wing, the next step is the aerodynamic analysis by using 3D Panel Method.

3.2 3D Panel Method

As it was mentioned before, 3D Panel Method is useful for obtaining C_P distribution around the airfoil, because is more accurate than other methods implemented, i.e. NLSM. This last method is easier to implement due to the singularities are placed in the plane $z = 0$, and for the method implemented they are placed on the surface of the wing. Besides, 3D Panel Method at LE provides a more detail C_P distribution.

This method is also accurate to compute the Critical Mach Number, but this is not an influence for the aerodynamic and structural analysis.

This method must be done without viscous effects because it is worked at high Reynolds numbers.

The results obtained in XFLR5 for the C_P distribution, are in incompressible flow, so it must be applied the Prandtl-Glauert compressibility correction, due to it is worked at subsonic compressible flow:

$$C_P^{(c)} = \frac{C_P^{(i)}}{\sqrt{1 - M_\infty^2}} \tag{3.1}$$

In some cases, Prandtl-Glauert correction can be neglected and assumed to be incompressible flow and therefore $C_P^{(i)}$ is valid. This validation is determined by the following conditions:

- $M \leq 0.3$
- Steady or quasisteady flow
- Isothermal

If these all conditions are satisfied, compressibility effects are small and either incompressible flow or compressible flow can be used. Therefore, it must be analysed the Mach number used in each flight phase. Although it happens in real cases, in the project is used compressibility effects for the entire flight.

In order to compute the value of the pressure difference, Bernoulli equation must be applied:

$$P = P_\infty + \frac{1}{2}\rho_\infty U_\infty^2 C_p^{(c)} \tag{3.2}$$

From this equation, the dynamic pressure is the one that is considered for the computation of the pressure difference between the total pressure and static pressure, because dynamic pressure is the one that generates the lift and drag forces.

At troposphere:

$$\rho_\infty = \rho_0(1 - 2.25569 \cdot 10^{-5}h)^{4.2561} \tag{3.3}$$

$$P_\infty = P_0(1 - 2.25569 \cdot 10^{-5}h)^{5.2561} \tag{3.4}$$

$$a_\infty = \sqrt{\gamma R T_\infty} = M_\infty\sqrt{\gamma R T_0(1 - 2.25569 \cdot 10^{-5}h)} \tag{3.5}$$

$$U_\infty = M_\infty a_\infty = M_\infty\sqrt{\gamma R T_\infty} = M_\infty\sqrt{\gamma R T_0(1 - 2.25569 \cdot 10^{-5}h)} \tag{3.6}$$

where $T_0 = 288.16K, P_0 = 101325\ Pa, \rho_0 = 1.225\ kg/m^3, \gamma = 1.4\ and\ R = 287\ m^2/s^2K$ and U_∞ is assumed to be True Airspeed.

Calling:

$$\theta = 1 - 2.25567 \cdot 10^{-5}h \tag{3.7}$$

Doing some substitutions and rearrangements equation (3.2) leads to:

$$P - P_\infty = \frac{\gamma P_0 \theta M_\infty^2 C_p^{(i)}}{2\sqrt{1 - M_\infty^2}} \tag{3.8}$$

It is appreciated that the pressure difference is a function that depends on the Mach number and the altitude, since the value of the pressure coefficient for incompressible flow is obtained directly from XFLR5 for all the points on the wing surface.

This formula must be used for all phases, so that it can be known in which phase the pressure is critical, so that it can be optimized the weight to have a lighter wing.

3.2.1 Take-off

During the take-off phase, the maximum speed reached is at the last phase of take-off (Steady climb). This phase is assumed to be at Sea Level conditions, so knowing that:

$$M_{TO} = \frac{V_2}{a} = \frac{1.2V_{stall}}{\sqrt{\gamma RT}} \tag{3.9}$$

where $V_{stall} = 68.33m/s$ and $a = 340.3\ m/s$ at S.L conditions, so the minimum result obtained is:

$$M_{TO} \geq 0.241$$

Therefore, there is a range of Mach values between the minimum one obtained and 0.3 in which compressibility corrections can be neglected for take-off phase.

As conclusion, $C_P^{(i)}$ can be used in this first phase, but it is not correct at all.

The wing is modelled with no high lift devices, like flaps at LE or TE. For instance, slats at LE are used as high lift devices for boundary layer control to reinject the flow or slotted flaps at TE to produce high lift. These devices are useful during take-off phase, because their absence does not produce enough lift and then leads to stall. As it was mentioned before, take-off is analysed in compressible regime.

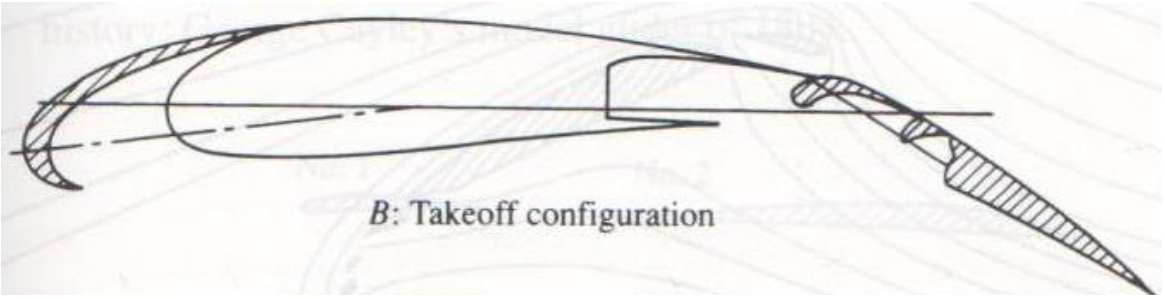

Figure 3.3 - Airfoil configuration during Takeoff [13]

In XFLR5, it cannot be created a model that has installed high-lift devices so it is designed as a simple wing. The problem of take-off must be solved by using CFD sources as Ansys, Fluent or OpenFoam in a range of Reynolds Numbers, and then retrieve those results for analysing the wing structurally in Abaqus. Nevertheless, it is solved using 3D Panel Method with XFLR5.

In any case, the contribution of the high-lift devices is subtracted due to the lift coefficient needed at take-off is very high and it happens at a high AoA, and it can lead to stall.

From equation (3.1) and (3.2), it can be appreciated that pressure difference at S.L. is:

$$P - P_0 = \frac{1}{2}\rho_0 {V_2}^2 \frac{C_P^{(i)}}{\sqrt{1 - M_{TO}^2}} \tag{3.10}$$

Equations of motion for take-off are:

$$L \geq W \tag{3.11}$$

$$\frac{1}{2}\rho_0 V_2^2 S C_L \geq MTOMg \tag{3.12}$$

Isolating the lift coefficient, equation (3.12) leads to:

$$C_L(\alpha) \geq \frac{2MTOMg}{\rho_0 S {V_2}^2} \tag{3.13}$$

When the AoA is obtained, the values of the pressure coefficient in incompressible flow are obtained, and can be substituted in equation (3.10).

3.2.2 Climb

For climb phase, flaps are not used as in take-off phase, so the configuration is the same as in cruise configuration and therefore it can be analysed as a normal configuration. Thus, there is no necessary to solve the problem using CFD software, it is solved using XFR5.

Firstly, it must be analysed the compressibility effects of the pressure distribution. Since aircraft is accelerating until reaching cruise phase and the speed of sound is decreasing at higher altitudes, there is a point in which reaches $M_{CL} \geq 0.3$. Thus, compressibility effects are considered.

$$L \geq W \cos\gamma \tag{3.14}$$

Since the pitch angle is very small:

$$\sin\gamma = \gamma \qquad \& \qquad \cos\gamma = 1 \tag{3.15}$$

Therefore equation (3.14) leads to equation (3.11), so applying the same steps as in equations of motion for take-off phase, the lift coefficient is:

$$C_L(\alpha) \geq \frac{2W}{\rho S V^2} = \frac{2MTOMg}{\rho(h) S M^2 a^2(h)} \tag{3.16}$$

where density and speed of sound are functions of the altitude, and the result of the lift coefficient during climbing is used to obtained the AoA and therefore, the pressure coefficient in incompressible flow as in take-off.

3.2.3 Cruise

In cruise phase, there is no flaps deployed so the configuration in this phase can be analysed using XFLR5, since do not disturb the pressure distribution around the airfoil. CFD sources can be discarded as well as in climb phase.

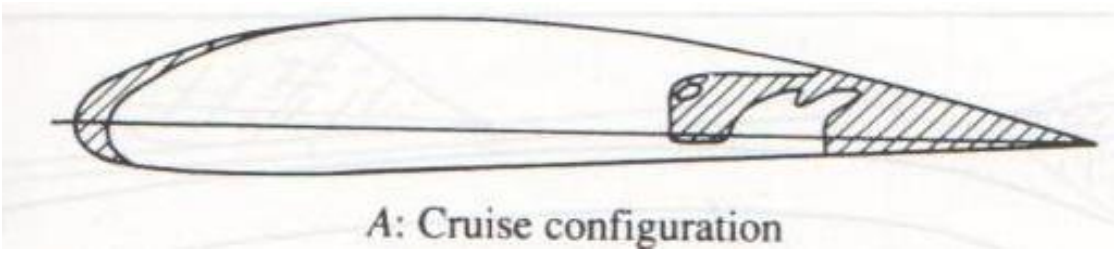

Figure 3.4 - Airfoil configuration during Cruise [13]

In this phase, it must be taken into account the altitude and speed of the aircraft to get an approximation of the pressure, and the initial and final weight, since the variation is the greatest in this phase.

The speed at this phase is greater and the speed of sound is smaller since it decreases with the altitude, so Mach number is $M_{CR} \geq 0.3$ and compressibility effects must be obtained for the calculation of pressure. The normal Mach number at cruise is $M_{CR} = 0.82$ and the maximum Mach at cruise is $M_{MO} = 0.86$. The Standard Regulations set these values at FL360, so the chosen analysis performed at that flight level is the normal Mach number.

On the other hand, the lift coefficient must be obtained to know at which angle of attack must fly the aircraft. Cruise is performed at steady level flight, so the equations of motion lead to:

$$L = W \tag{3.17}$$

$$\frac{1}{2}\rho(h)V_{CR}^2 S C_L = W \tag{3.18}$$

$$C_L(\alpha) = \frac{2W}{\rho(h)SV_{CR}^2} = \frac{2MTOMg}{\rho(h)SM_{CR}^2 a^2(h)} \tag{3.19}$$

3.2.4 Descent

Same thing occurs as in climb phase:

- No flaps (normal configuration)
- Compressible flow ($M_{DC} \geq 0.3$)

The equations used for climbing are the same for descending. Just the MTOM changes to a value close to MLM, since the most part of fuel is consumed at cruise and cannot lands at a higher value.

3.2.5 Landing

It must be considered that during landing, the maximum value of Mach number occurs at the approaching phase, and must be:

$$M_{LD} \geq \frac{1.3V_{stall}}{a} \tag{3.20}$$

The same conditions are applied as in take-off, the S.L. conditions and the values of the speed of sound and stall speed. The minimum Mach number obtained is:

$$M_{LD} \geq 0.261$$

If it is assumed that the final approach is in a range of this value and $M = 0.3$, then incompressible flow can be applied and no Prandtl Glauert compressibility correction can be used. But, it is assumed for all phases the use of compressible flow.

As in take-off, the flaps are deployed to have a lower stall speed and makes the aircraft lands in a shorter distance. This situation generates the same problem as in first phase, where flaps are not assumed in XFLR5, so it can be analysed in a better way using CFD sources at a range of Reynolds numbers.

Finally, for this last phase, the equations of motion used are the same as used in Take-off, but in this case changes the MTOM to MLW and V_2 to V_{app}, so:

$$C_L(\alpha) \geq \frac{2MTOMg}{\rho_0 S V_{app}^2} \tag{3.21}$$

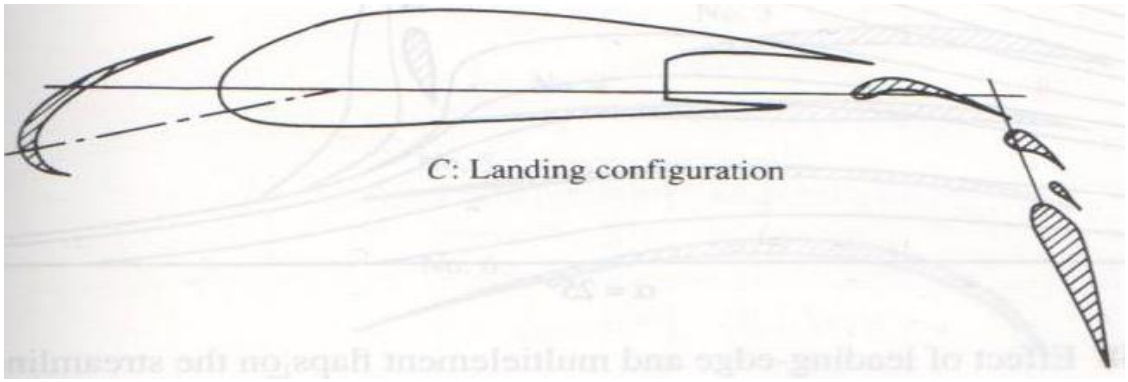

Figure 3.5 - Airfoil configuration during Landing [13]

3.3 Results

All the above equations for all the phases, must be used to compute the lift coefficient needed for the aircraft performances. After taking those values, the results of the AoA can be computed from $C_L vs\ \alpha$ graph. The AoA obtained provide the computation of each C_P in incompressible flow for all the panels. Therefore, the pressure difference can be computed and finally can be used as an input for the structural analysis. The $C_L\ vs\ \alpha$ obtained in XFLR5 using 3D panel method is the following one:

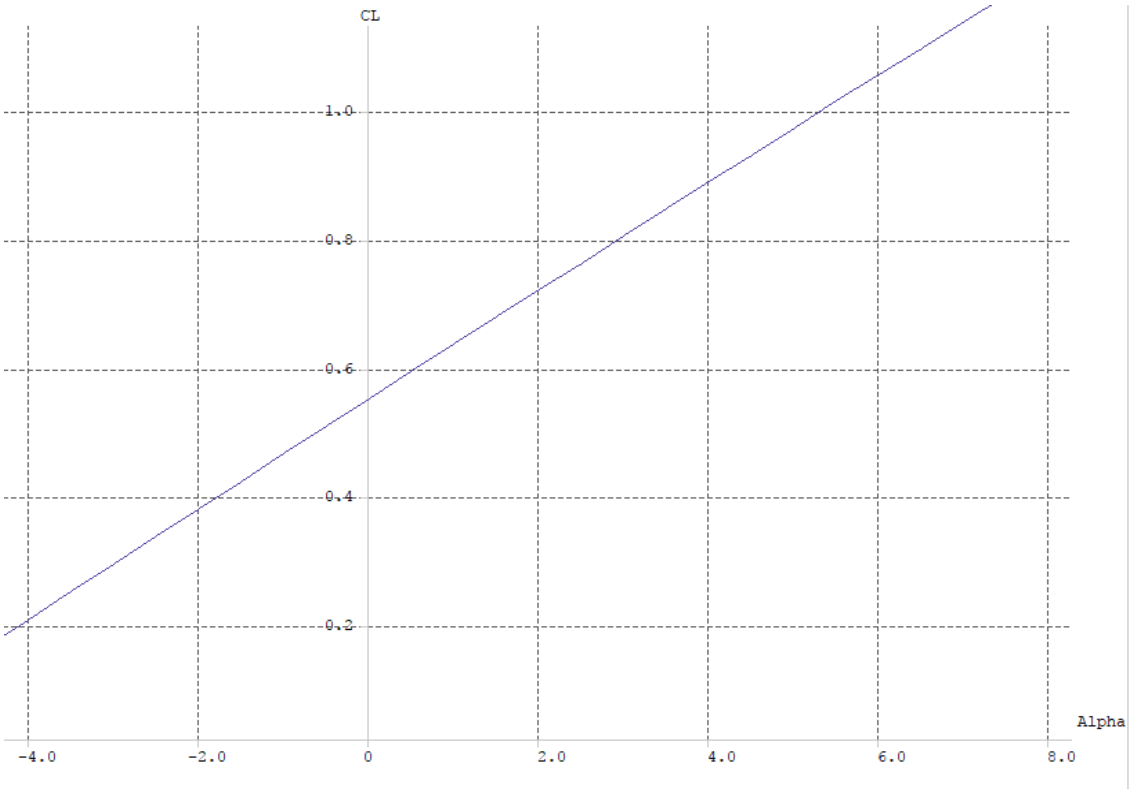

Figure 3.6 – Lift coefficient vs Angle of Attack

Since density and speed of sound decreases as altitude increases, it must be set the values at those altitudes that standard regulations have established, therefore to compute density and speed of sound, equation (3.3) is used because it is necessary these values for the computation of the lift coefficient:

Altitude(ft//m)	***Density(kg/m^3)***	***Speed of sound(m/s)***
0//0	1.225	340.3
10000//3048	0.9046	328.4
24000//7315	0.5686	311.0
36000//11000	0.3652	295.1

Table 3.2 - Density and Speed of sound as a function of Altitude

In the case that the values provided from the standard regulations for the speed of the aircraft are different from TAS, i.e. IAS, CAS, EAS, they must be converted through these equations:

$$V_{CAS} = V_{IAS} + \Delta e \tag{3.21}$$

$$V_{EAS} = f V_{CAS} \tag{3.22}$$

$$V_{TAS} = \frac{V_{EAS}}{\sqrt{\sigma}} \tag{3.23}$$

Since standard regulations do not provide the position error, it is assumed that the indicated airspeed and the calibrated airspeed are the same, so equations (3.21), (3.22) and (3.23) leads to:

$$V_{TAS} = \frac{f V_{IAS}}{\sqrt{\sigma}} \tag{3.24}$$

where f is the compressibility correction factor and σ is the density ratio.

h	Calibrated Airspeed (knots)										
ft	100	125	150	175	200	225	250	275	300	325	350
0	1	1	1	1	1	1	1	1	1	1	1
5000	0.9994	0.9991	0.9987	0.9983	0.9978	0.9972	0.9966	0.9959	0.9952	0.9944	0.9936
10000	0.9987	0.9980	0.9971	0.9961	0.9950	0.9938	0.9924	0.9909	0.9893	0.9876	0.9859
15000	0.9978	0.9966	0.9952	0.9935	0.9916	0.9895	0.9872	0.9848	0.9822	0.9794	0.9766
20000	0.9967	0.9949	0.9927	0.9902	0.9874	0.9842	0.9809	0.9773	0.9735	0.9695	0.9654
25000	0.9953	0.9927	0.9896	0.9860	0.9820	0.9777	0.9730	0.9681	0.9629	0.9575	0.9520
30000	0.9934	0.9898	0.9856	0.9807	0.9754	0.9695	0.9633	0.9568	0.9500	0.9430	0.9359
35000	0.9910	0.9862	0.9805	0.9741	0.9670	0.9594	0.9513	0.9429	0.9343	0.9256	0.9167
36089	0.9904	0.9852	0.9792	0.9724	0.9649	0.9568	0.9483	0.9395	0.9305	0.9213	0.9121
40000	0.9879	0.9815	0.9740	0.9657	0.9565	0.9468	0.9367	0.9263	0.9157	0.9051	
45000	0.9840	0.9757	0.9661	0.9555	0.9441	0.9321	0.9197	0.9071	0.8947		
50000	0.9793	0.9686	0.9565	0.9433	0.9293	0.9148	0.9001	0.8858			

Figure 3.7 - Compressibility factor from CAS to EAS [14]

All the pressure difference values obtained from Bernoulli, must be multiplied by a Safety Factor of 2.5 for all phases, even though the Federal Aviation Regulations at section 25.303 has established a Factor of Safety of 1.5.

3.3.1 Take-off

To compute the lift coefficient, it must be known that high lift devices increases lift in a mean value of 75%. Thus, the value obtained must be divided into 1.75. Substituting in equation (3.12), and knowing that $\rho_0 = 1.225\ kg/m^3$, $S = 437.3m^2$, $MTOM = 368000\ kg$, $V_2 = 82\ m/s$ and $g = 9.80665\ m/s^2$, the results for both C_L and α (from Figure 3.6) and M_{TO} from equation (3.9) are:

	$M_{TO}(-)$	$C_L\ (-)$	$\alpha(deg)$
@h=0ft=0m	*0.241*	*1.143*	*7.0*

Table 3.3 - Mach number, Lift coefficient and AoA during Take-off

Therefore, it is obtained a set of pressure coefficient values for each panel of the wing at that AoA in incompressible flow. Applying equation (3.8) at the altitude corresponding to this phase and using the Factor of Safety, the pressure difference results obtained at the upper and lower surfaces are represented below in Tables 3.4 and 3.5, and it can be seen that higher values at lower and upper surfaces occur close to the tip at LE.

PRESSURE AT LOWER SURFACE (Pa) @M=0.241								
	ROOT							***TIP***
TE	*2516.0*	*2561.4*	*2606.0*	*2617.6*	*2599.3*	*2573.6*	*2463.7*	*1259.3*
	2114.9	*2223.8*	*2346.0*	*2453.6*	*2508.9*	*2519.7*	*2436.5*	*1011.0*
	1756.6	*2034.1*	*2330.9*	*2611.2*	*2803.8*	*2892.9*	*2894.2*	*1544.3*
LE	*2590.0*	*3086.4*	*3480.5*	*3747.7*	*3873.7*	*3882.4*	*3615.0*	*2674.0*

Table 3.4 - Pressure difference at lower surface during Take-off phase

PRESSURE AT UPPER SURFACE (Pa) @M=0.241								
	ROOT							***TIP***
LE	*-9449.6*	*-11564.6*	*-13533.9*	*-15476.6*	*-16960.5*	*-17608.9*	*-18384.8*	*-16381.1*
	-11550.3	*-12652.7*	*-13685.8*	*-14697.1*	*-15356.7*	*-15552.5*	*-15795.1*	*-13526.9*
	-6984.3	*-7305.0*	*-7731.7*	*-8170.9*	*-8382.3*	*-8456.1*	*-8443.5*	*-6824.8*
TE	*-1257.9*	*-1276.8*	*-1394.0*	*-1525.1*	*-1562.3*	*-1591.9*	*-1544.5*	*-1119.1*

Table 3.5 - Pressure difference at upper surface during Take-off phase

3.3.2 Climb

In climb phase, two altitude points are studied established by standard regulations. First it is necessary to compute each Mach number at these two altitudes. Then, using equation (3.16) and Table 3.2, lift coefficient and AoA can be obtained. [15]

1) From 0 ft to 10000 ft (FL100), $V_{TAS} \leq 250\ kts = 128.61\ m/s$
2) Up to 24000 ft (240FL), $V_{IAS} \leq 290\ kts = 149.19\ m/s$

The first Mach number can be obtained using equation (3.6) and table 3.2.

The second Mach number is obtained:

- First by converting the indicated airspeed to true airspeed through equation (3.24).
- Second by using equation (3.6) and table 3.2.

From figure 3.7, the compressibility factor is obtained by interpolation, so the value at FL240 is $f = 0.96698$. The density ratio is $\sigma = 0.46416$. Then, $V_{TAS} = 411.6\ kts = 211.75\ m/s$. Therefore, the results obtained are:

	$\boldsymbol{M_{CL}(-)}$	$\boldsymbol{C_L\ (-)}$	$\boldsymbol{\alpha(deg)}$
@h=10kft=3048m	*0.395*	*1.103*	*6.9*
@h=24kft=7315m	*0.680*	*0.647*	*1.1*

Table 3.6 - Mach number, Lift coefficient and AoA during Climb

Now, pressure differences are obtained through equation (3.8) for these two altitudes at each Mach number at upper and lower surfaces, and applying Factor of Safety. In Tables 3.7 and 3.9, it can be seen that values at the middle of the wing in the lower surfaces are exposed to higher forces at the Leading Edge. At the upper surfaces, the higher values are close to the tip at LE.

PRESSURE AT LOWER SURFACE (Pa) @M=0.395								
	ROOT							TIP
TE	5977.0	6068.1	6157.8	6181.0	6144.3	6092.7	5871.9	3451.3
	5171.0	5389.8	5635.4	5851.5	5962.8	5984.3	5817.1	2952.4
	4450.7	5008.5	5605.0	6168.3	6555.3	6734.5	6737.1	4024.1
LE	6125.6	7123.3	7915.4	8452.3	8705.6	8723.0	8185.6	6294.5

Table 3.7 - Pressure difference at lower surface during Climb phase (1)

PRESSURE AT UPPER SURFACE (Pa) @M=0.395								
	ROOT							TIP
LE	-18070.8	-22321.4	-26279.2	-30183.5	-33165.8	-34468.8	-36028.0	-32001.3
	-22292.5	-24508.1	-26584.3	-28616.8	-29942.4	-30335.9	-30823.5	-26264.9
	-13116.1	-13760.7	-14618.1	-15500.9	-15925.8	-16074.0	-16048.7	-12795.6
TE	-1607.6	-1645.7	-1881.1	-2144.7	-2219.3	-2279.0	-2183.6	-1328.6

Table 3.8 - Pressure difference at upper surface during Climb phase (1)

PRESSURE AT LOWER SURFACE (Pa) @M=0.680								
	ROOT							TIP
TE	8977.7	9163.5	9286.2	9267.6	9186.9	9104.5	8848.8	7141.0
	5599.8	5956.7	6255.2	6479.9	6616.0	6649.4	6534.3	4478.0
	572.4	1237.4	1944.4	2621.3	3161.2	3511.5	3775.0	1995.7
LE	-6266.8	-4402.2	-2244.4	-169.0	1493.8	2534.6	3519.8	1686.0

Table 3.9 - Pressure difference at lower surface during Climb phase (2)

PRESSURE AT UPPER SURFACE (Pa) @M=0.680								
	ROOT							TIP
LE	-10883.0	-13878.0	-16419.5	-18826.0	-20637.4	-21386.9	-22395.7	-20232.9
	-28031.0	-30246.4	-32125.3	-33888.6	-34953.8	-35067.0	-35167.7	-30257.8
	-19382.6	-20030.5	-20867.3	-21709.5	-22021.6	-22014.9	-21780.9	-17180.2
TE	-2601.6	-2566.8	-2788.1	-3073.5	-3130.8	-3168.7	-3019.7	-1015.5

Table 3.10 - Pressure difference at upper surface during Climb phase (2)

3.3.3 Cruise

Cruise phase is performed by regulations at $M_{CR} = 0.82$ [15], so using this value and equation (3.19), the results are:

	$M_{CR}(-)$	$C_L\,(-)$	$\alpha(deg)$
@h=36kft=11000m	*0.82*	*0.775*	*2.7*

Table 3.11 - Mach number, Lift coefficient and AoA during Cruise

And therefore, the pressure difference at cruising for both surfaces are:

PRESSURE AT LOWER SURFACE (Pa) @M=0.82								
	ROOT							***TIP***
TE	*11565.2*	*11787.0*	*11958.0*	*11964.1*	*11874.6*	*11774.3*	*11411.4*	*8412.8*
	8255.5	*8715.5*	*9149.6*	*9502.0*	*9702.6*	*9753.2*	*9546.5*	*5887.6*
	3752.8	*4742.3*	*5795.4*	*6800.0*	*7553.0*	*7986.0*	*8229.3*	*4799.3*
LE	*814.4*	*3494.3*	*6232.7*	*8709.4*	*10541.7*	*11520.1*	*12126.1*	*8860.6*

Table 3.12 - Pressure difference at lower surface during Cruise phase

Table 3.13 shows higher values a

PRESSURE AT UPPER SURFACE (Pa) @M=0.82								
	ROOT							***TIP***
LE	*-20940.4*	*-26140.6*	*-30778.8*	*-35270.1*	*-38683.3*	*-40142.9*	*-41956.7*	*-37556.0*
	-39020.6	*-42386.1*	*-45373.1*	*-48232.7*	*-50024.0*	*-50377.6*	*-50770.7*	*-43454.1*
	-25438.4	*-26425.3*	*-27718.3*	*-29033.7*	*-29587.5*	*-29681.2*	*-29459.9*	*-23247.3*
TE	*-3403.6*	*-3399.8*	*-3748.2*	*-4168.9*	*-4266.9*	*-4338.7*	*-4143.0*	*-1746.9*

Table 3.13 - Pressure difference at upper surface during Cruise phase

It must be taken into account that at the end of this phase, the most part of the fuel weight is used so descent phase is performed at a value close to MLW.

3.3.4 Descent

Same thing happens as climb phase, two points are analysed at the same altitudes, and the steps for achieving the values of the lift coefficient and the AoA are the same. [15]

1) From FL360 to FL240, $M_{DC} = 0.81$
2) From FL240 to FL100, reducing speed to $V_{IAS} = 290kts = 149.19\,m/s$

Since the first Mach number is provided, the second Mach number is computed applying the same steps as in climb phase, using equation (3.6) and table 3.2.

Interpolating the compressibility factor @FL240, it is obtained that $f = 0.98994$. The density ratio is $\sigma = 0.73847$. Finally, $V_{TAS} = 334\ kts = 171.82\ m/s$. Thus, the following results are:

	$M_{DC}(-)$	$C_L\,(-)$	$\alpha(deg)$
@h=10kft=3048m	0.523	0.436	-1.3
@h=24kft=7315m	0.81	0.323	-2.7

Table 3.14 - Mach number, Lift coefficient and AoA during Descent

And the pressure difference with factor of safety for both altitudes are:

PRESSURE AT LOWER SURFACE (Pa) @M=0.81								
	ROOT							***TIP***
TE	16534.4	16907.2	17072.5	16930.8	16729.9	16552.2	16167.3	14754.6
	7358.8	7967.1	8314.5	8488.0	8626.4	8639.3	8566.8	7341.5
	-7795.5	-7139.7	-6449.2	-5779.9	-5091.8	-4478.7	-3841.5	-3773.3
LE	-42521.9	-41686.8	-39290.1	-36566.1	-33855.2	-31418.2	-28528.9	-27672.2

Table 3.15 - Pressure difference at lower surface during Descent phase (1)

PRESSURE AT UPPER SURFACE (Pa) @M=0.81								
	ROOT							***TIP***
LE	-4139.9	-7031.1	-8956.4	-10551.7	-11657.3	-11989.8	-12910.5	-12465.0
	-42354.7	-45092.6	-47071.8	-48790.0	-49678.9	-49385.4	-48988.5	-42974.6
	-33186.9	-33960.0	-34904.2	-35813.7	-35979.5	-35706.6	-35105.0	-28022.9
TE	-4107.7	-3936.7	-4174.0	-4549.3	-4588.2	-4603.6	-4366.7	-786.1

Table 3.16 - Pressure difference at upper surface during Descent phase (1)

PRESSURE AT LOWER SURFACE (Pa) @M=0.523								
	ROOT							***TIP***
TE	8723.6	8915.0	9018.5	8970.6	8877.1	8790.3	8568.3	7458.5
	4575.5	4912.3	5148.0	5300.6	5403.6	5424.6	5355.4	4130.9
	-2011.9	-1516.2	-991.6	-486.6	-39.3	298.4	608.0	-151.8
LE	-14693.4	-13495.1	-11722.2	-9892.7	-8280.1	-7075.7	-5739.0	-6416.9

Table 3.17 - Pressure difference at lower surface during Descent phase (2)

PRESSURE AT UPPER SURFACE (Pa) @M=0.523								
	ROOT							TIP
LE	-5620.4	-7667.3	-9240.5	-10659.1	-11699.4	-12092.2	-12756.1	-11774.5
	-24612.0	-26363.5	-27745.2	-29000.5	-29713.1	-29668.3	-29581.5	-25679.3
	-18199.0	-18705.2	-19342.8	-19972.2	-20154.2	-20068.6	-19786.1	-15675.3
TE	-2372.8	-2307.0	-2472.4	-2705.4	-2740.6	-2760.7	-2624.9	-657.8

Table 3.18 - Pressure difference at upper surface during Descent phase (2)

3.3.5 Landing

Finally, the main data for landing phase are $MLW = 259000\ kg$, $V_{app} = 88.83\ m/s$ and all the at S.L., so using equation (3.21) and table 3.2, leads to:

	$M_{LD}(-)$	$C_L\ (-)$	$\alpha(deg)$
@h=0ft=0m	0.261	1.202	7.0

Table 3.19 - Mach number, Lift coefficient and AoA during Landing

The results obtained for pressure difference applying Factor of Safety at Landing phase are:

PRESSURE AT LOWER SURFACE (Pa) @M=0.261								
	ROOT							TIP
TE	3030.0	3083.2	3135.5	3149.1	3127.7	3097.5	2968.7	1556.0
	2559.6	2687.3	2830.6	2956.8	3021.7	3034.3	2936.7	1264.9
	2139.3	2464.8	2812.9	3141.6	3367.5	3472.1	3473.6	1890.3
LE	3116.7	3699.0	4161.2	4474.6	4622.4	4632.5	4318.9	3215.3

Table 3.20 - Pressure difference at lower surface during Landing phase

PRESSURE AT UPPER SURFACE (Pa) @M=0.261								
	ROOT							TIP
LE	-11004.0	-13484.6	-15794.4	-18072.9	-19813.3	-20573.7	-21483.7	-19133.8
	-13467.8	-14760.8	-15972.5	-17158.6	-17932.2	-18161.9	-18446.4	-15786.1
	-8112.5	-8488.7	-8989.1	-9504.3	-9752.2	-9838.7	-9823.5	-7925.5
TE	-1396.3	-1418.5	-1555.9	-1709.7	-1753.3	-1788.1	-1732.1	-1233.5

Table 3.21 - Pressure difference at upper surface during Landing phase

Results obtained in Tables 3.20 and 3.21 are like 3.4 and 3.5, because when Bernoulli equation is applied, the density is the same at S.L, and speed are very similar for both phases.

Chapter 4

Numerical Structural Analysis

The forth chapter consists on performing numerical structural analysis by Finite Element Method. It is analysed through Abaqus/CAE software and it follows three main steps, pre-processing, processing and post-processing, as it was explained in section 2.3.2. The main goal is achieving a light wing without failure, so before starting the analysis, failure criteria is explained in the first section of this chapter. After showing the main concepts of failure, the maximum displacement in the vertical axis is considered for the analysis. Finally, the description of the wing design and optimization procedure is presented.

4.1 Failure Criteria

Different failure criteria are used to study the behaviour of the materials in such a way that do not reach the corresponding failure conditions associated to each material. Two different materials are used during the structural analysis, isotropic and composite, each of them with different failure criteria.

- Isotropic material: Mechanical and thermal properties are the same in all directions. This kind of materials are focused on the elastic region in such a way that does not reach yield stress. Von Mises criterion is used for this material.
- Composite material: Layers of composite materials are laminar or sandwich, so, from laminate theory, it is known that the behaviour of these materials is anisotropic. Hashin criterion is applied in this material.

4.1.1 Von Mises criterion

If the material is ductile and isotropic does not have to reach yield stress, because if it exceeds elastic region the material will present a plastic behaviour, so it is considered failure. Von Mises criterion defines the VM stress to be the maximum allowable stress, which is the yield stress. VM criterion is defined by the following formula, in which $\sigma_1, \sigma_2, \sigma_3$ are the stresses in the three principal directions:

$$\sigma_y \geq \sigma_{VM} = \sqrt{\frac{1}{2}[(\sigma_{11} - \sigma_{22})^2 + (\sigma_{11} - \sigma_{33})^2 + (\sigma_{22} - \sigma_{33})^2]} \tag{4.1}$$

When an isotropic material is used, the maximum value that appears in the post-processing step using Von Mises criterion corresponds to the yield stress, so the material must not reach that value, since it will have exceeded the elastic region.

4.1.2 Hashin criterion

This criterion is used for composite materials, which are usually composed by fiber and matrix, and they have anisotropic behaviour. It studies failure during compression or tension, for both fiber and matrix. Hashin criterion defines these four cases with the following equations:

$$d_{fc}^2 = \frac{\sigma_{11}}{X_C} \tag{4.2}$$

$$d_{ft}^2 = \left(\frac{\sigma_{11}}{X_T}\right)^2 + \alpha\left(\frac{\sigma_{12}^2 + \sigma_{13}^2}{S_L^2}\right) \tag{4.3}$$

$$d_{mc}^2 = \frac{1}{Y_C}\left[\left(\frac{Y_c}{2S_T}\right)^2 - 1\right](\sigma_{22} + \sigma_{33}) + \left(\frac{\sigma_{22} + \sigma_{33}}{2S_T}\right)^2 + \frac{\sigma_{23}^2 + \sigma_{22}\sigma_{33}}{S_T^2} + \frac{\sigma_{12}^2 + \sigma_{13}^2}{S_L^2} \tag{4.4}$$

$$d_{mt}^2 = \left(\frac{\sigma_{22} + \sigma_{33}}{Y_T}\right)^2 + \left(\frac{\sigma_{12}^2 + \sigma_{13}^2}{S_L^2}\right) + \left(\frac{\sigma_{23}^2 - \sigma_{22}\sigma_{33}}{S_T^2}\right)^2 \tag{4.5}$$

Equations (4.2) and (4.4) relates compression for matrix and fiber, and equations (4.3) and (4.5) relates tension for matrix and fiber. For avoiding failure in this criterion, maximum values must be less than one when FEM is used. It means that, principal stresses must not exceed all longitudinal and transverse stresses for tension and compression.

Compression is linked with buckling and crushing, so equation (4.2) express the relationship between buckling and fiber compression, where is only considered the longitudinal compressive stress, and equation (4.4) links matrix compression with crushing using transverse compressive stress.

Tension is taken into account by the study of fiber breakage and it is related with the longitudinal tensile stress in equation (4.3). The matrix tension is optimized to prevent cracking, so using equation (4.5), it can be appreciated that is related to transverse tensile stress.

4.2 Vertical displacement

The maximum vertical displacement is computed due to wing can present aerodynamic losses or vibration problems, and therefore there must be studied the maximum swept angle. The percentage of displacement is the maximum displacement divided by the semispan, and it cannot exceed twenty percent.

4.3 Pre-processing

As it was explained in section 2.3.2, the pre-processing step is used to define the wing, the materials used, loads around the wing, mesh… It covers from part module to mesh module, so each module is analysed independently. In this step, pre-processing englobes the complete wing design process.

4.3.1 Part Module

- **Airfoil Section**

In order to model the NACA 6415 airfoil, coordinates from table 3.1 are defined in Abaqus, obtaining the following figure.

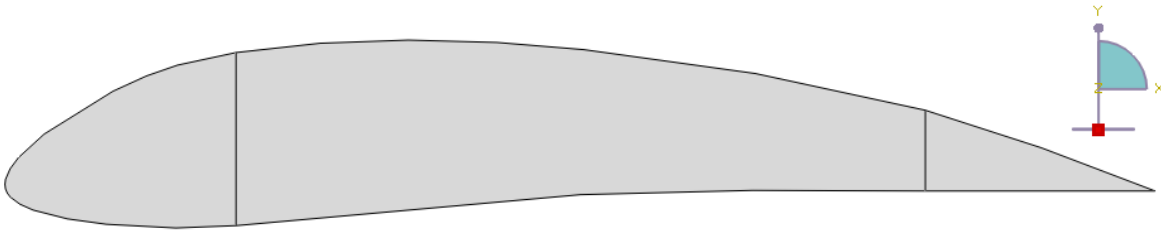

Figure 4.1 – NACA 6415 Foil using Abaqus/CAE

It is seen that there are two partitions in this section. These lines are used to define two spars of the wing located at 20% and 80% of the chord from LE.

Ribs are represented by the shape of the airfoil. The wing is divided into nine different ribs, and the distances between them along the span, are proportional w.r.t the initial rib, located at the root of the wing. Thus, nine different parts are created in this module.

Although distances between ribs are proportional, it does not mean that the rib sizes are proportional, since TE is not linearly constant and changes along the span, so the chord value of each rib is computed by interpolation. Therefore, it is obtained that:

	Rib 1	***Rib 2***	***Rib 3***	***Rib 4***	***Rib 5***	***Rib 6***	***Rib 7***	***Rib 8***	***Rib 9***
Chord (m)	*12.18*	*10.723*	*9.2713*	*7.8151*	*6.363*	*5.4375*	*4.515*	*3.592*	*2.67*

Table 4.1 - Chord length of each Rib

Each value is multiplied by the coordinates of Table 3.1 to get points of all airfoils at real scale, so that nine ribs can be obtained as NACA 6415.

4.3.2 Assembly Module

- **Wing section**

This module is used to create the assembly of the wing:

The first step has consisted on joining the nine parts created in the first module, in such a way that the position in Z-axis between ribs was proportional from root to tip, and the position in X-axis w.r.t to LE of the first rib was determined by:

$$X_n = Z_n \tan(\Lambda_{\mathrm{LE}}) \tag{4.6}$$

where Λ_{LE} is the swept angle and X_n and Z_n represents the position of each rib (n=1, …, 9) in both axis at LE. Therefore, as $\Lambda_{LE} = 31.1\ deg$, the results obtained are:

	Rib 1	**Rib 2**	**Rib 3**	**Rib 4**	**Rib 5**	**Rib 6**	**Rib 7**	**Rib 8**
$\boldsymbol{Z_n(m)}$	3.965	7.931	11.897	15.862	19.828	23.794	27.759	31.725
$\boldsymbol{X_n(m)}$	2.392	4.784	7.177	9.569	11.961	14.353	16.746	19.138

Table 4.2 - Position at X-axis and Z-axis of the LE of each rib w.r.t. Rib 1 LE

Points mentioned above, are used to locate the different ribs in the correct position along the span. The rib distribution of the wing is shown in Figure 4.2.

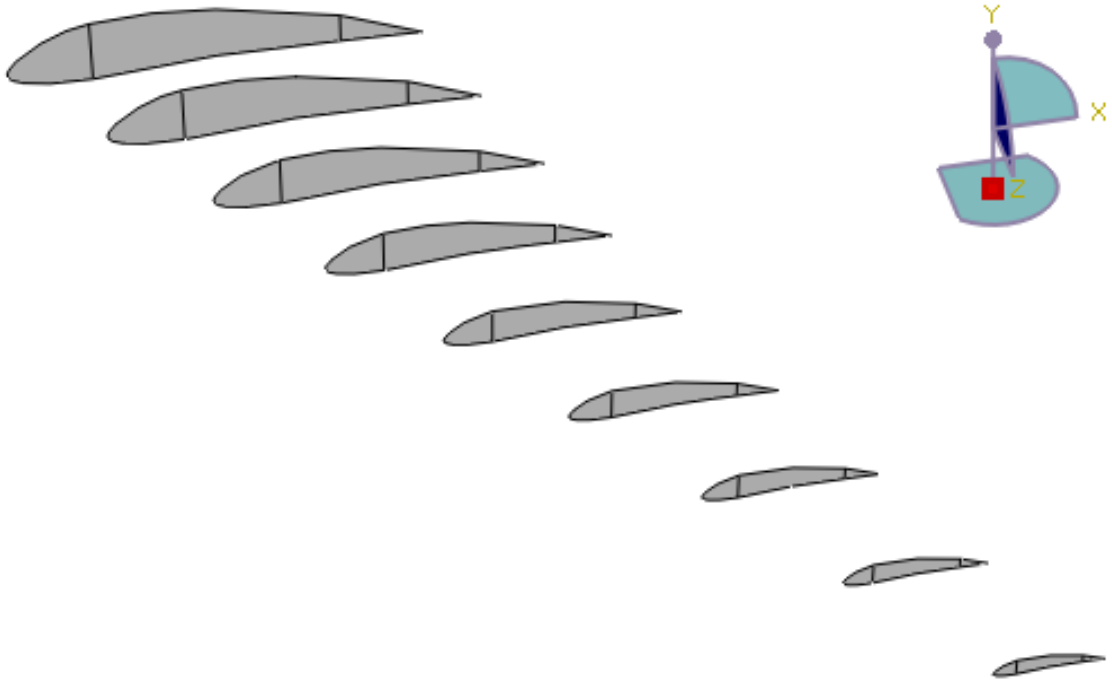

Figure 4.2 – Representation of the position of the ribs inside the wing

The next step consisted on modelling the wing internally and externally, starting from spars and finishing with the skin surface.

For the spar modelling, the partitions created at the ribs are used to extrude these aircraft component. Figure below shows the rib distribution with spars.

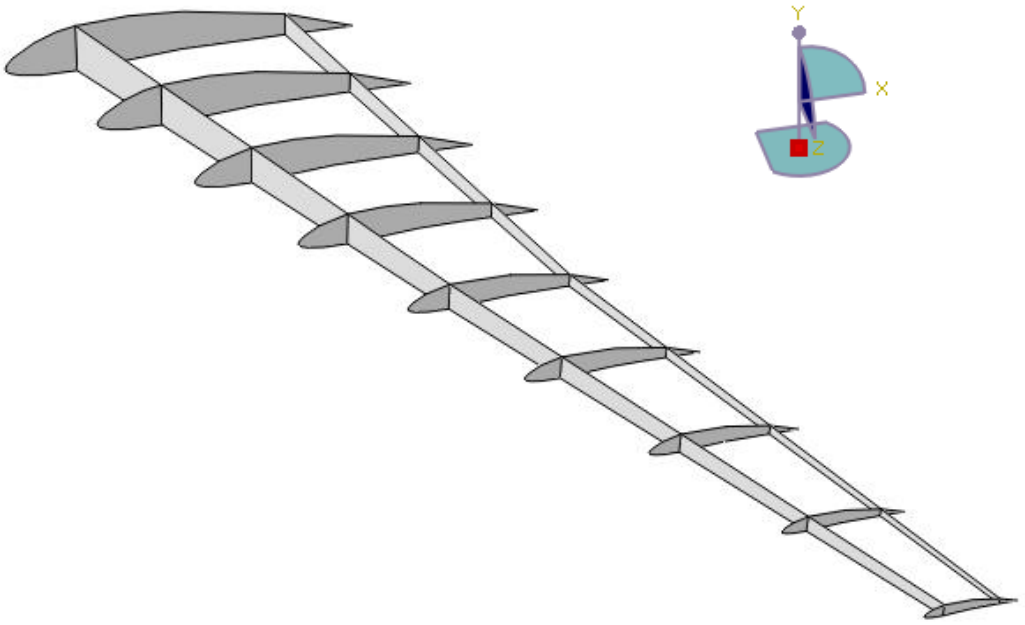

Figure 4.3 – Spars and Ribs defining the wing internal structure

After modelling the internal structure of the wing, the external part of the wing is created to cover both spars and ribs at the upper and lower surfaces.

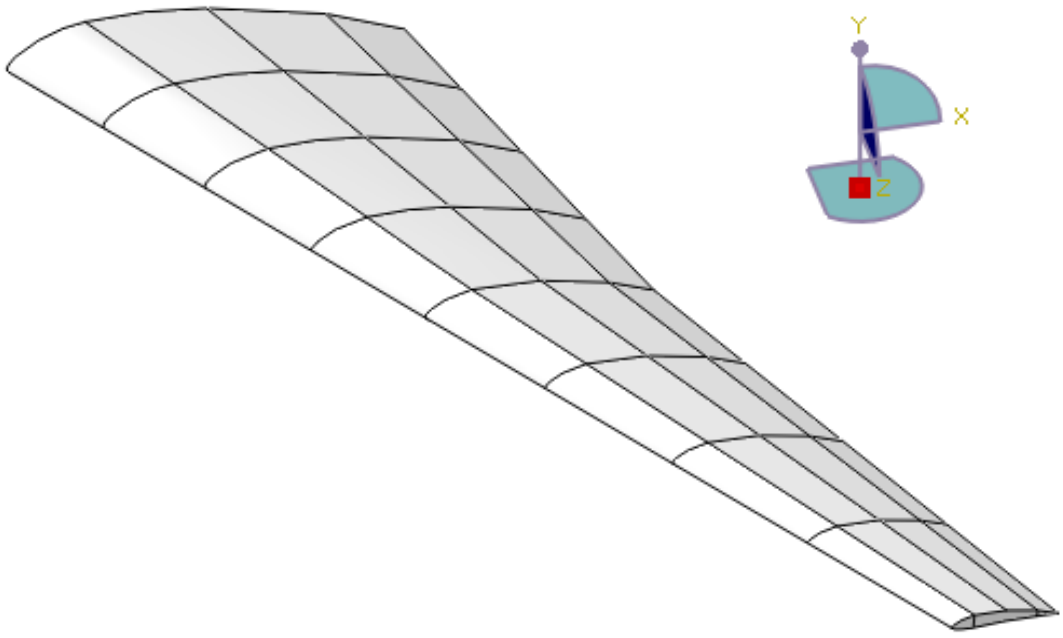

Figure 4.4 – A340 600 Wing structure

4.3.3 Step Module

This module is used to choose the kind of analysis and the results to visualize in the post-processing step. VM criteria (isotropic material), Hashin criteria (composite material) and the maximum vertical displacement are selected as an output in this module in order to have them available after finishing the analysis.

4.3.4 Load Module

In this module, it is introduced all pressures obtained in aerodynamic analysis for all flight phases.

First of all, it is defined the Boundary Conditions at the wing. It is known that the wing behaves as a clamped beam due to it is attached to the fuselage, so displacements and rotations in all axes are restricted at the wing root.

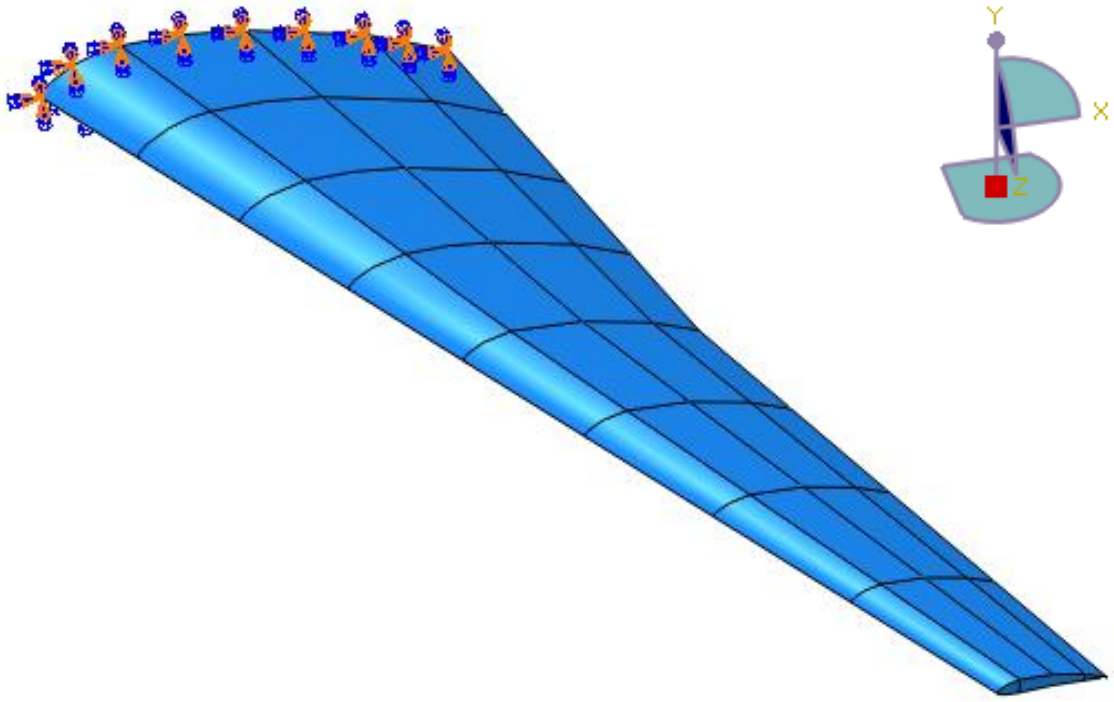

Figure 4.5 - Encastre at wing root

Then, pressures obtained in the numerical aerodynamic analysis, are introduced in Abaqus to perform the numerical structural analysis for all flight phases. They are introduced perpendicular to the panels, at the same way as they were obtained.

To know in which panel is introduced difference pressure values from section 3.3, in Figure 4.6 it is represented an organization of the panels with pressure. At the upper surface, it is composed of four panels chordwise from TE to LE and eight panels spanwise from root to tip, as shown in tables for upper part. The lower part only is differenced chordwise, changing from LE to TE, as depicted in tables for lower surfaces.

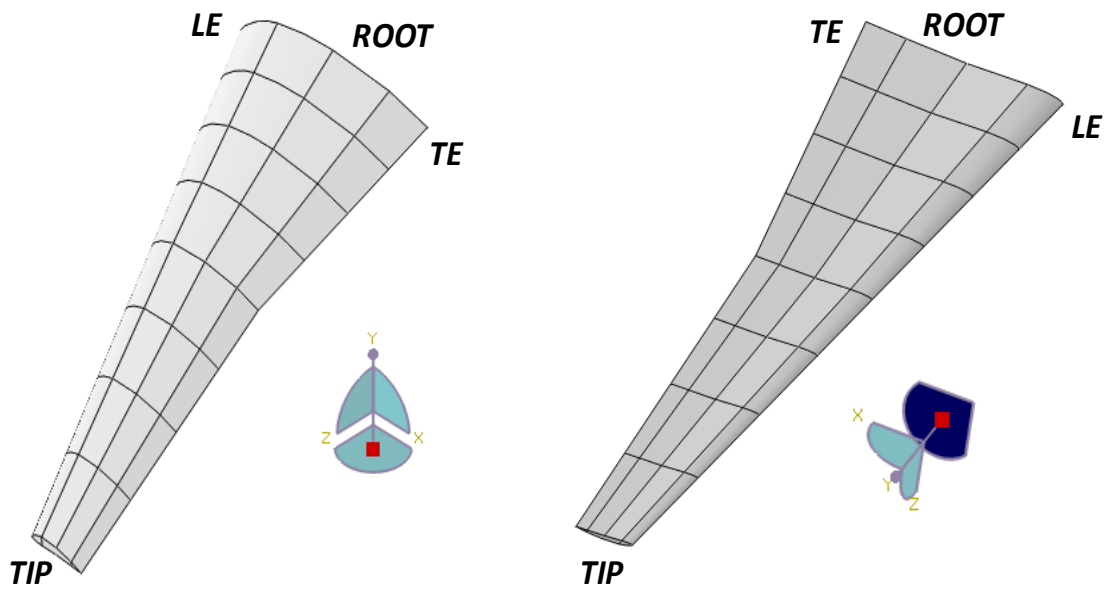

Figure 4.6 – Upper Surface (left) and Lower Surface (right) of the wing

After knowing the distribution of the values of pressure difference in all panels, they are introduced in the Load Module as a mechanical category and pressure as a type for selected step. So, five different models are created for each flight phase. During climb and descent phases, it is introduced the most critical loads for each phase.

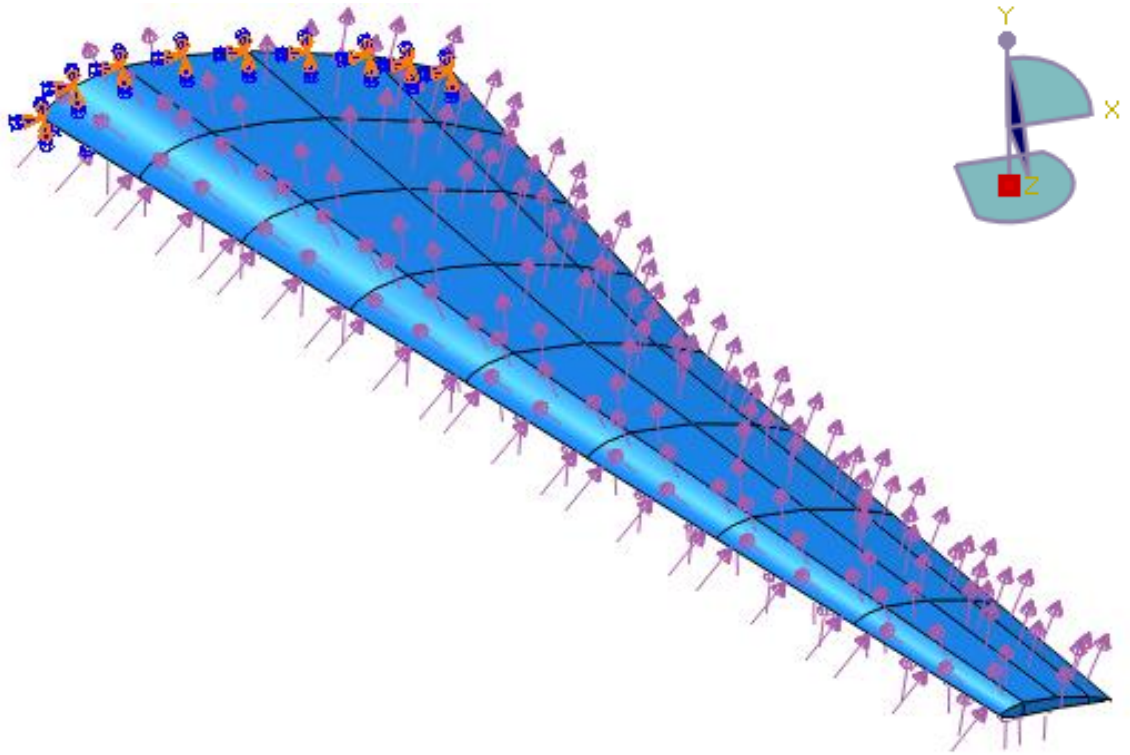

Figure 4.7 - Load distribution along the chord and the span at upper and lower surfaces

4.3.5 Mesh Module

This module is used to discretize the wing in finite elements applying FEM. The model is meshed using both quadrilateral and triangular elements.

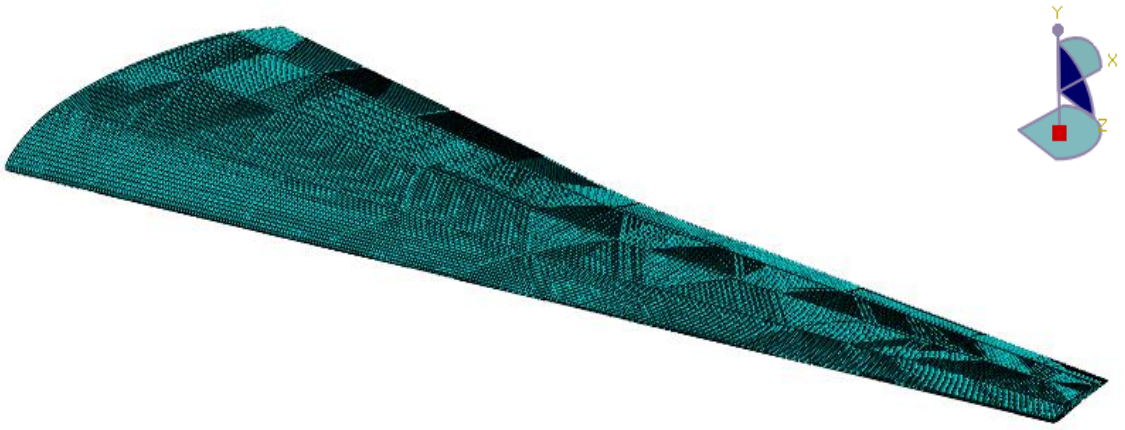

Figure 4.8 - Wing skin meshing using quadrilateral elements

The external structure of the wing is only composed of quadrilateral elements, and the internal structure is composed of quadrilateral elements at the spars and at the center part of the ribs, and sections forming LE and TE are composed of both triangular and quadrilateral elements, as it is shown in Figure 4.9.

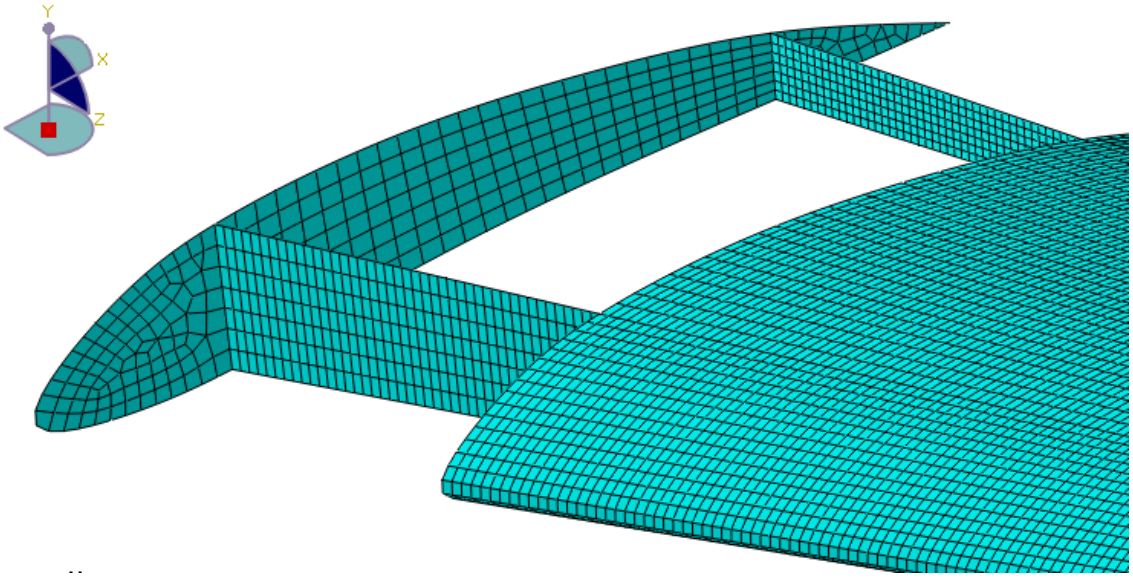

Figure 4.9 - Ribs, spars and skin meshing using both quadrilateral and triangular elements

The total number of nodes and elements (quadrilateral and triangular) obtained are:

Number of nodes	Number of elements	Quadrilateral elements	Triangular elements
44204	45390	45340	50

Table 4.3 - Mesh main data

4.3.6 Property Module

The materials and the divided sections of the wing are defined in this module. This part works as a feedback, because it is used to optimize the wing weight in such a way that does not fail, depending on the criterion applied and the thickness used in each section.

As it was mentioned in section 4.1, two materials are studied for the optimization. The first one is isotropic and ductile, so, Al 7075-T6 is the material selected to apply VM criterion. The second one is composite and the material used is Carbon Fiber Epoxy MTM45-1. These two materials are commonly used in aeronautics.

The main properties of these materials are depicted in these tables below:

$\boldsymbol{\rho\ (kg/m^3)}$	$\boldsymbol{\sigma_y(MPa)}$	$\boldsymbol{E(GPa)}$	$\boldsymbol{\nu\ (-)}$
2810	503	72	0.33

Table 4.4 - Main properties of Al 7075-T6 [16]

$\boldsymbol{\rho\ (kg/m^3)}$	1600
$\boldsymbol{E_1(GPa)}$	162
$\boldsymbol{E_2(GPa)}$	7.93
$\boldsymbol{G_{12}(GPa)}$	5.3
$\boldsymbol{G_{13}(GPa)}$	5.3
$\boldsymbol{G_{23}(GPa)}$	4
$\boldsymbol{\nu(-)}$	0.35
$\boldsymbol{X_T(MPa)}$	2899
$\boldsymbol{X_C(MPa)}$	1414
$\boldsymbol{Y_T(MPa)}$	37
$\boldsymbol{Y_C(MPa)}$	169
$\boldsymbol{S_L(MPa)}$	134
$\boldsymbol{S_T(MPa)}$	120

Table 4.5 - Main properties of Carbon Fiber Epoxy MTM45-1 [17]

Now, skin sections are divided in LE and TE. Each one, is divided in upper and lower part and they are divided in which one section is composed of 4 panels with the shape of a square, starting from root and finishing at tip. In Figure 4.10, it can be seen the representation of TEup1 and LEdown3.

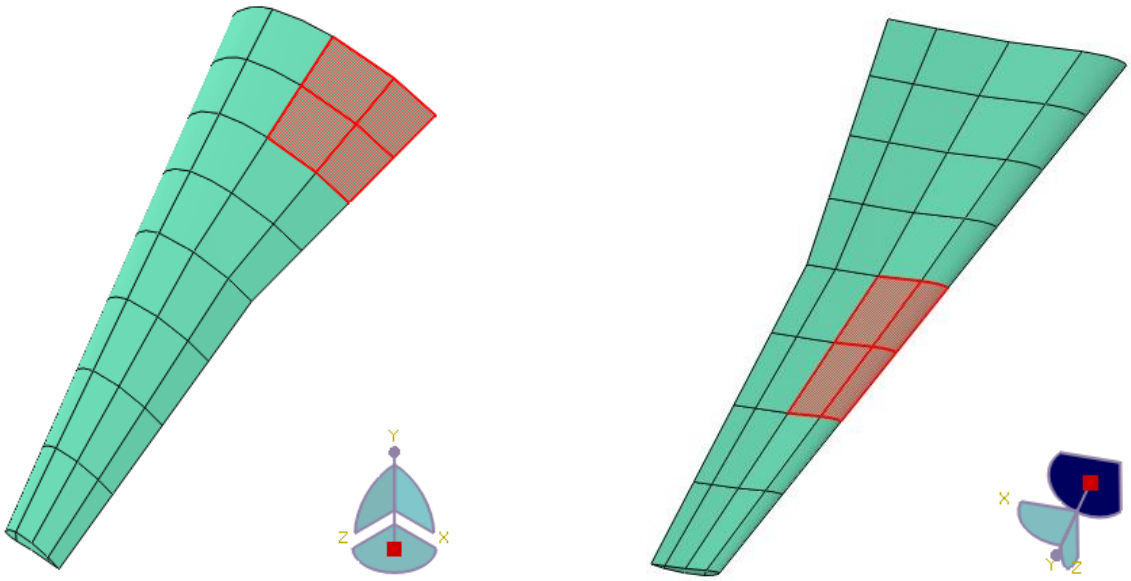

Figure 4.10 - TEup1 (left) and LEdown3 (right) sections

Moreover, spars are divided into front spar (FS) and rear spar(RS), and these two are divided at inside and outside. Ribs are taken in pairs, except Rib1, which is at the root.

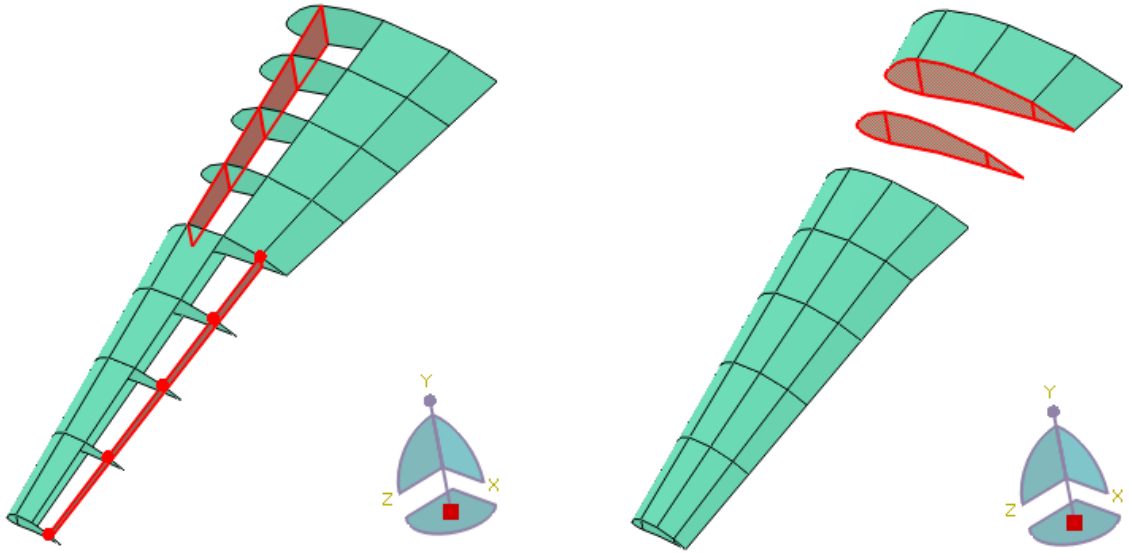

Figure 4.11 – FSin and RSout (left), and Rib23 (right) sections

4.4 Processing

4.4.1 Job Module

Once pre-processing step is finished, Job module is used to execute the program so that it is visualised the results chosen in Step Module.

4.5 Post-processing

4.5.1 Visualization Module

In the last step, results are divided into two sections. The first part is a comparison between all flight phases using Al 7075-T6, and then, the most critical phase is taken using VM theory. The second part is a comparison between the isotropic material and the composite one mentioned above, at the same critical flight phase.

4.6 Results

As it was said in visualization module, the first part of the results is shown for Al 7075-T6 for all flight phases, so it is depicted below VM maximum stresses and maximum displacements and the minimum weight.

4.6.1 Take-off

For take-off analysis, pressures shown in Tables 3.4 and 3.5 at Load Module, and thicknesses used are:

	LEup (mm)	LEdown (mm)	TEup (mm)	TEdown (mm)
Section 1	7	7	7	6
Section 2	7	7	4.5	5
Section 3	6	5	3.5	4
Section 4	3	3	2	1.5

Table 4.6 - Thicknesses using Al 7075-T6 at different skin sections during Take-off

	FrontSpar (mm)	RearSpar (mm)
Inside	4	4
Outside	4	1

Table 4.7 - Thicknesses using Al 7075-T6 at spars during Take-off

Rib 1 (mm)	Rib23 (mm)	Rib 45 (mm)	Rib 67 (mm)	Rib 89 (mm)
0.5	8	6	1.5	1

Table 4.8 - Thicknesses using Al 7075-T6 at Ribs during Take-off

After this optimization, the results obtained are:

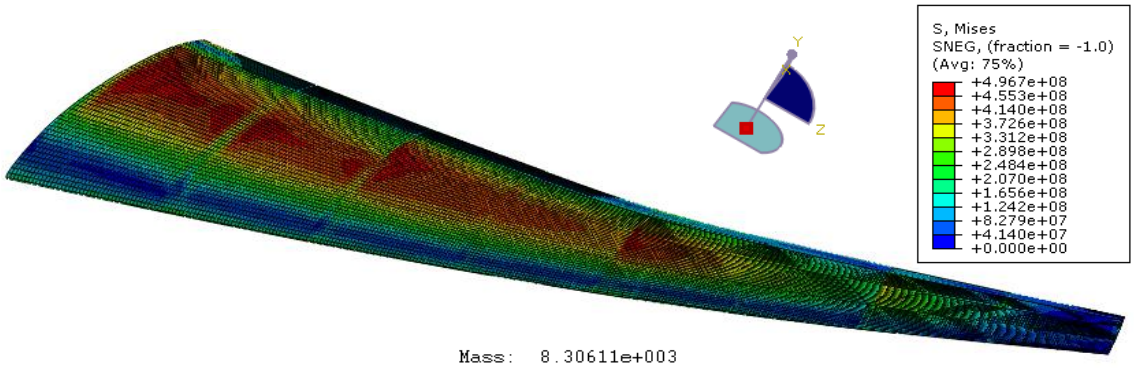

Figure 4.12 - Von Mises stresses during Take-off

As it is shown in Figure 4.12, maximum VM stress is obtained in the upper panel near the wing root, because the region near the root are subjected to higher stresses. As it is shown in Tables 4.6, 4.7 and 4.8 thicknesses used in this region are higher in order to withstand these higher stresses.

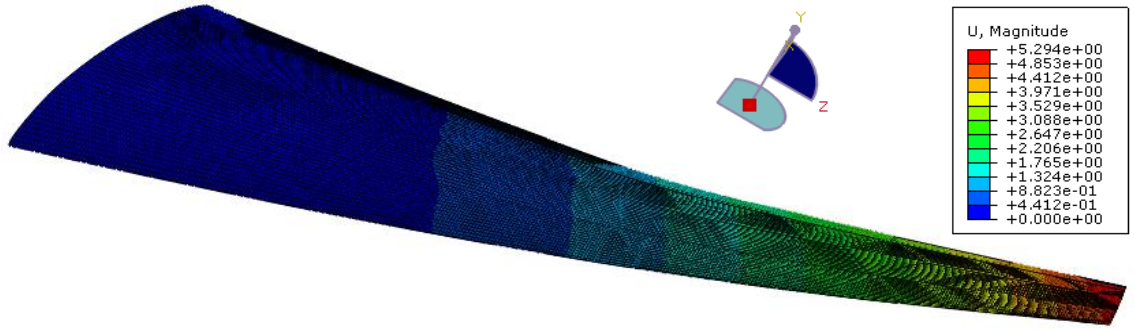

Figure 4.13 - Displacements during Take-off

The minimum weight and maximum VM stress and displacement for Take-off are:

$\sigma_{VM}(MPa)$	$U_{max}(m)$	$M_{min}(kg)$
496.7	5.294	8306.1

Table 4.9 - Results during Take-off

4.6.2 Climb

During climb phase, the chosen case to analyse is the second one, then, Tables 3.9 and 3.10 are taken to introduce the pressure values at Load module. Thicknesses obtained for climb phase after optimizing are:

	LEup (mm)	LEdown (mm)	TEup (mm)	TEdown (mm)
Section 1	12.5	12.5	15	15
Section 2	12.5	10	10	10
Section 3	11.5	10	6	9
Section 4	5	5	4	4

Table 4.10 - Thicknesses using Al 7075-T6 at different skin sections during Climb

	FrontSpar (mm)	RearSpar (mm)
Inside	20	17.5
Outside	10	1.5

Table 4.11 - Thicknesses using Al 7075-T6 at spars during Climb

Rib 1 (mm)	Rib23 (mm)	Rib 45 (mm)	Rib 67 (mm)	Rib 89 (mm)
0.5	4.5	3	2.5	1.5

Table 4.12 - Thicknesses using Al 7075-T6 at Ribs during Climb

Then, the results obtained during climb are:

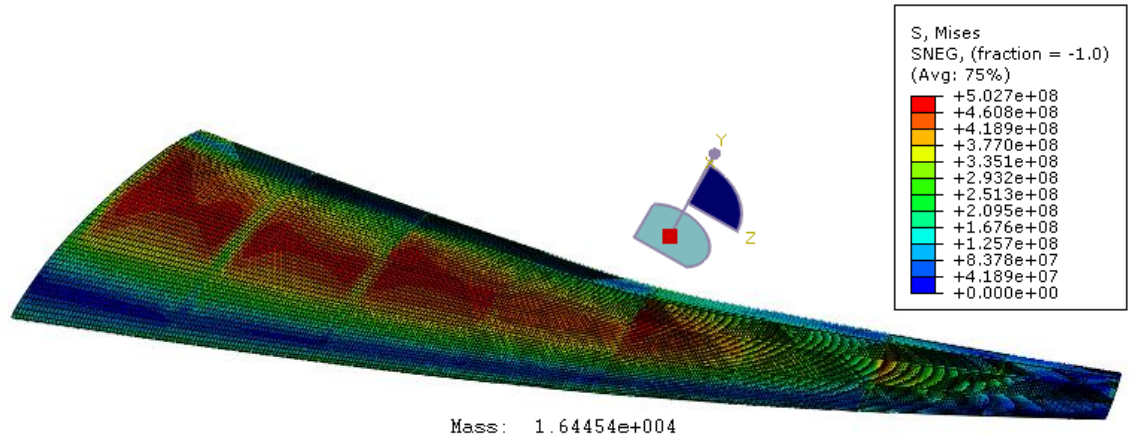

Figure 4.14 - Von Mises stresses during Climb

For the same reason, higher stresses are located close to wing root

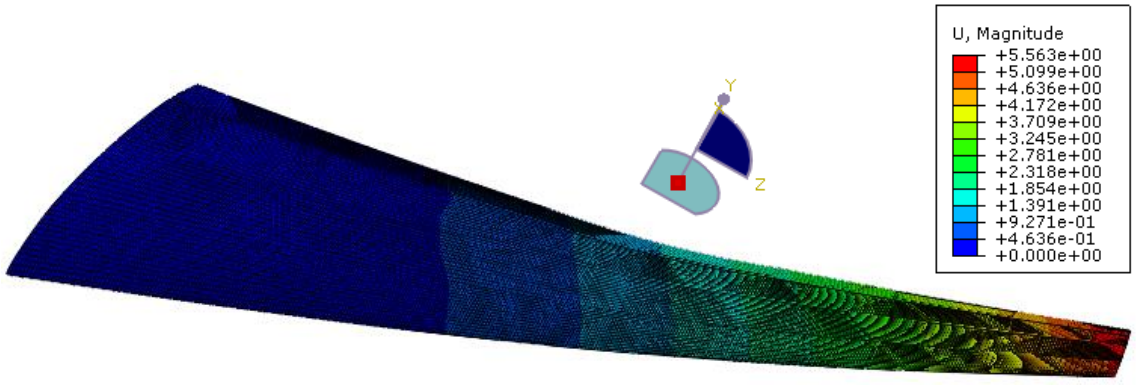

Figure 4.15 - Displacements during Climb

Displacements are higher at the tip due to the bending moment because it is a free end.

The results obtained for minimum weight, and maximum VM stress and displacement are:

$\sigma_{VM}(MPa)$	$U_{max}(m)$	$M_{min}(kg)$
502.7	5.563	16445.4

Table 4.13 - Results during Climb

4.6.3 Cruise

Cruise phase is performed with Tables 3.12 and 3.13, when normal cruise Mach number is reached. Thicknesses obtained, when normal cruise Mach is used to optimize, are:

	LEup (mm)	LEdown (mm)	TEup (mm)	TEdown (mm)
Section 1	23	12.5	22	23
Section 2	21	12.5	17.5	17.5
Section 3	20	12.5	12.5	12.5
Section 4	7	5	6	4

Table 4.14 - Thicknesses using Al 7075-T6 at different skin sections during Cruise

	FrontSpar (mm)	RearSpar (mm)
Inside	20	17.5
Outside	10	2.5

Table 4.15 - Thicknesses using Al 7075-T6 at spars during Cruise

Rib 1 (mm)	Rib23 (mm)	Rib 45 (mm)	Rib 67 (mm)	Rib 89 (mm)
0.5	4.5	3	1.5	1

Table 4.16 - Thicknesses using Al 7075-T6 at Ribs during Cruise

It is appreciated that thicknesses are greater in this phase than in take-off and climb. This is because dynamic pressure is the greatest and it is necessary thicker skin, spars and ribs to withstand it.

So, the results are for VM stresses are:

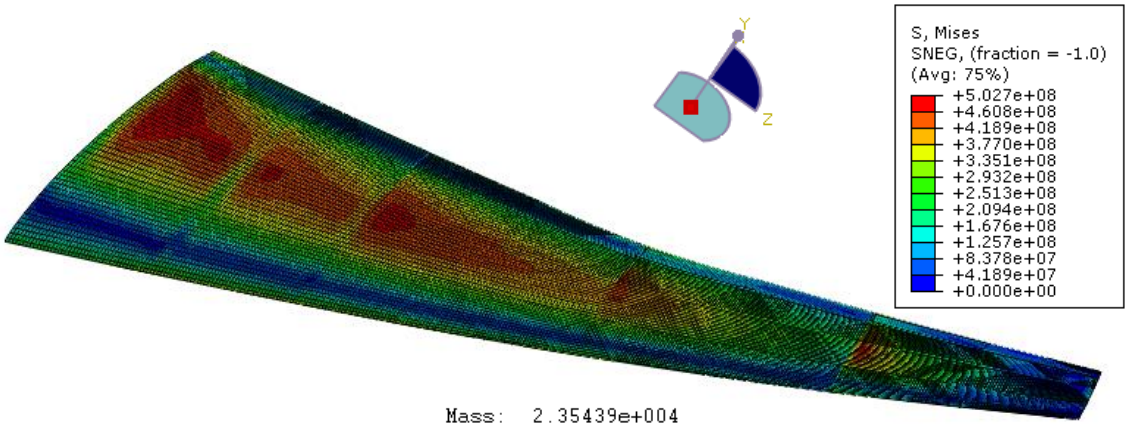

Figure 4.16 - Von Mises stresses during Cruise

As take-off and climb, Von Mises stresses during Cruise are higher at the upper skin near to the wing root due to it is subjected to higher stresses. Since it is necessary thicker sections, the weight is higher and the most restrictive.

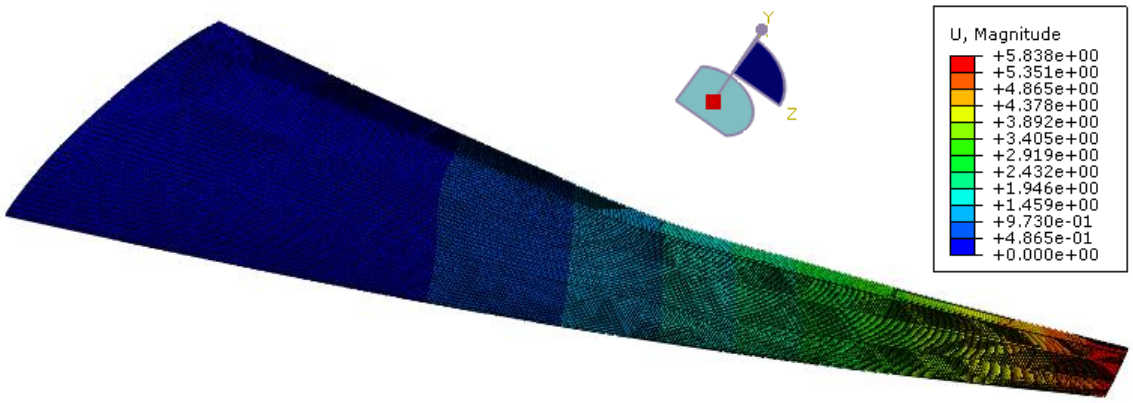

Figure 4.17 - Displacements during Cruise

Displacements are higher at the tip because it is a free end and the moment is greater.

The minimum weight and maximum VM stress and displacement for Cruise are:

$\sigma_{VM}(MPa)$	$U_{max}(m)$	$M_{min}(kg)$
502.7	5.838	23543.9

Table 4.17 - Results during Cruise

4.6.4 Descent

Same thing happens as climb phase. Since there are two different phases during descent, only one is chosen for the analysis. It is chosen the critical one, where the values are higher. Therefore, it is used Tables 3.15 and 3.16, where the Mach number is greater, and the results can be appreciated that are higher than pressures at Tables 3.17 and 3.18. First, the values of thicknesses obtained for the optimization during descent phase are:

	LEup (mm)	LEdown (mm)	TEup (mm)	TEdown (mm)
Section 1	15	12.5	15	15
Section 2	15	12.5	9	10
Section 3	12.5	12.5	7	9
Section 4	7	5	6	4

Table 4.18 - Thicknesses using Al 7075-T6 at different skin sections during Descent

	FrontSpar (mm)	RearSpar (mm)
Inside	20	17.5
Outside	10	1.5

Table 4.19 - Thicknesses using Al 7075-T6 at spars during Descent

Rib 1	Rib23	Rib 45	Rib 67	Rib 89
0.5	4.5	3	2.5	1.5

Table 4.20 - Thicknesses using Al 7075-T6 at Ribs during Descent

Von Mises stresses during descent phase are:

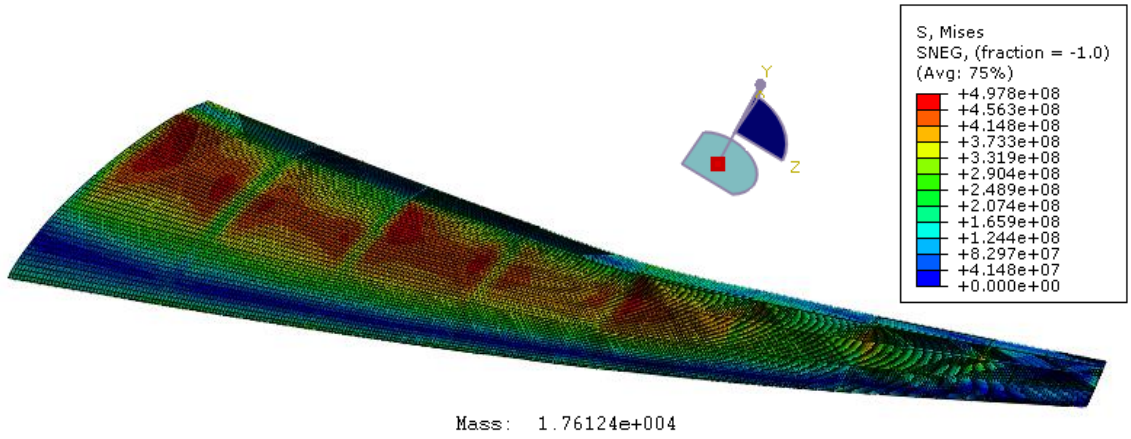

Figure 4.18 - Von Mises stresses during Descent

In Figure 4.18, maximum stresses in descent phase are close to wing as in all phases. Thinner sections are used in this phase to withstand forces, so the minimum weight is not the more restrictive, since it still is cruise phase.

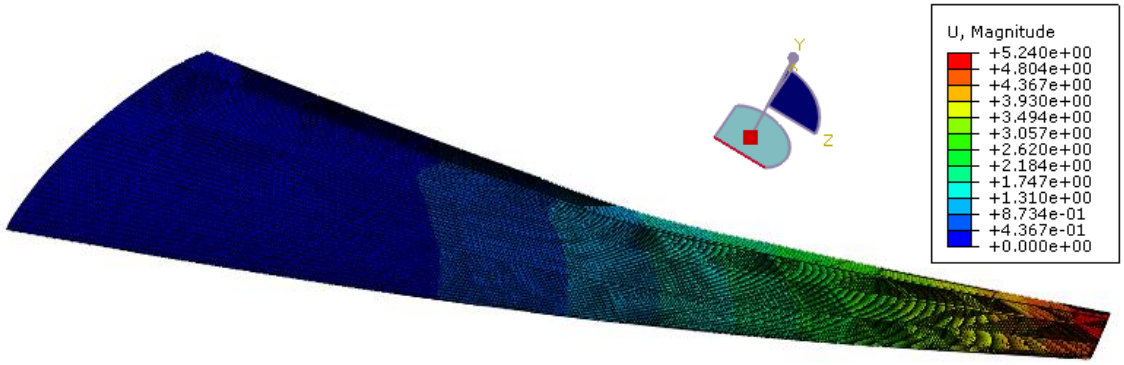

Figure 4.19 - Displacements during Descent

Same distribution of the displacements as in all phases but lower displacements than in cruise phase because the pressure difference values are lower.

The minimum weight and maximum VM stress and displacement for Descent are:

$\sigma_{VM}(MPa)$	$U_{max}(m)$	$M_{min}(kg)$
497.8	5.240	17612.4

Table 4.21 - Results during Descent

4.6.5 Landing

Finally, pressure from Tables 3.20 and 3.21 are used for landing phase. Thicknesses used for optimization are similar to take-off since dynamic pressure values are close, so the following thicknesses are:

	LEup (mm)	LEdown (mm)	TEup (mm)	TEdown (mm)
Section 1	15	12.5	15	15
Section 2	15	12.5	9	10
Section 3	12.5	12.5	7	9
Section 4	7	5	6	4

Table 4.22 - Thicknesses using Al 7075-T6 at different skin sections during Landing

	FrontSpar (mm)	RearSpar (mm)
Inside	20	17.5
Outside	10	1.5

Table 4.23 - Thicknesses using Al 7075-T6 at spars during Landing

Rib 1	Rib23	Rib 45	Rib 67	Rib 89
0.5	4.5	3	2.5	1.5

Table 4.24 - Thicknesses using Al 7075-T6 at Ribs during Landing

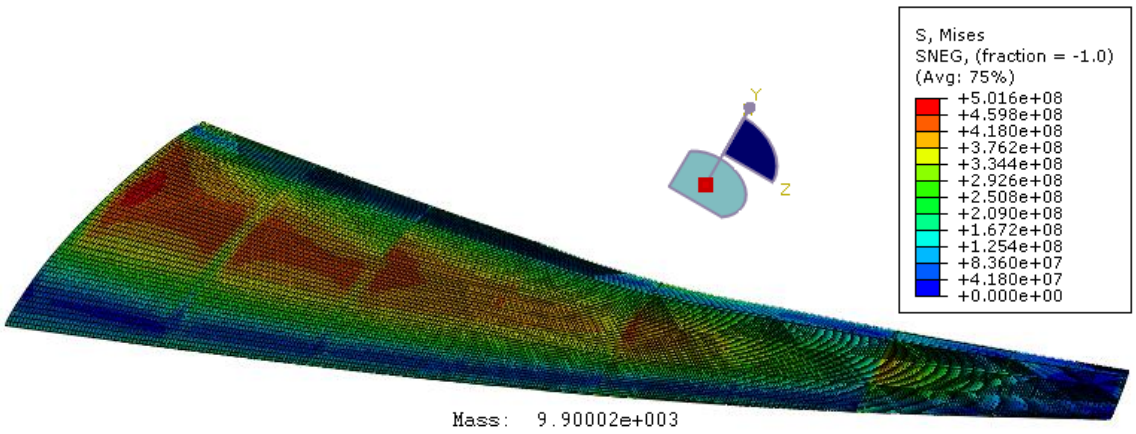

Figure 4.20 - Von Mises stresses during Landing

The results obtained are the same as all phases and the wing has less weight

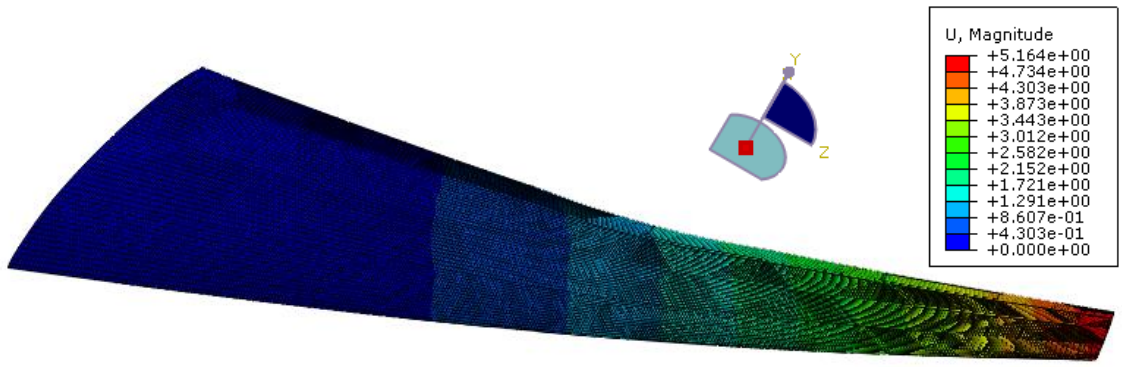

Figure 4.21 - Displacements during Landing

Free end condition produces the same result as in all flight phases for the displacement.

Finally, during landing thinner sections are used than sections at descent phase, so a lighter wing is obtained

The minimum weight and maximum VM stress and displacement for Landing are:

$\sigma_{VM}(MPa)$	$U_{max}(m)$	$M_{min}(kg)$
501.6	5.164	9900.0

Table 4.25 - Results during Landing

The results obtained for each phase are summarized in Table 4.10 so that it can be checked the critical phase.

	$\sigma_{VM}(MPa)$	$U_{max}(m)$	$M_{min}(kg)$
Take-off	496.7	5.294	8306.1
Climb	502.7	5.563	16445.4
Cruise	502.7	5.838	23543.9
Descent	497.8	5.240	17612.4
Landing	501.6	5.164	9900.0

Table 4.26 - Summary of results for all phases using Al 7075-T6

Thus, Cruise phase is the most critical, since the minimum weight is the highest one when the values of Von Mises stresses are close to yield stress. Therefore, Cruise phase is taken for the optimization using different materials.

4.7 Optimization using different materials

In this section, it is compared the results obtained for Al-7075-T6 and Carbon Epoxy MTM45-1 during Cruise phase, since it is the critical one.

4.7.1 Al 7075-T6

As it was depicted above, Table 4.4 is used to introduce the Al 7075-T6 property data and the results obtained for Von Mises are shown in Figure 4.16. The thicknesses at skin, spars and ribs used to obtain these results covers all flight phases, and are the following ones:

	LEup (mm)	LEdown (mm)	TEup (mm)	TEdown (mm)
Section 1	23	12.5	22	23
Section 2	21	12.5	17.5	17.5
Section 3	20	12.5	12.5	12.5
Section 4	7	5	6	4

Table 4.27 - Final thicknesses using Al 7075-T6 at different skin sections

	FrontSpar (mm)	RearSpar (mm)
Inside	20	17.5
Outside	10	2.5

Table 4.28 – Final thicknesses using Al 7075-T6 at spars

Rib 1	Rib23	Rib 45	Rib 67	Rib 89
0.5	4.5	3	1.5	1

Table 4.29 – Final thicknesses using Al 7075-T6 at Ribs

4.7.2 Carbon Epoxy MTM45-1

This material is analysed through Hashin criterion for cruise phase as Al 7075-T6, so the property data at Table 4.5 is introduced, and the maximum results obtained for Fiber tension and compression (HSNFCCRT and HSNFTCRT), and Matrix tension and compression (HSNMCCRT and HSNMTCRT), are:

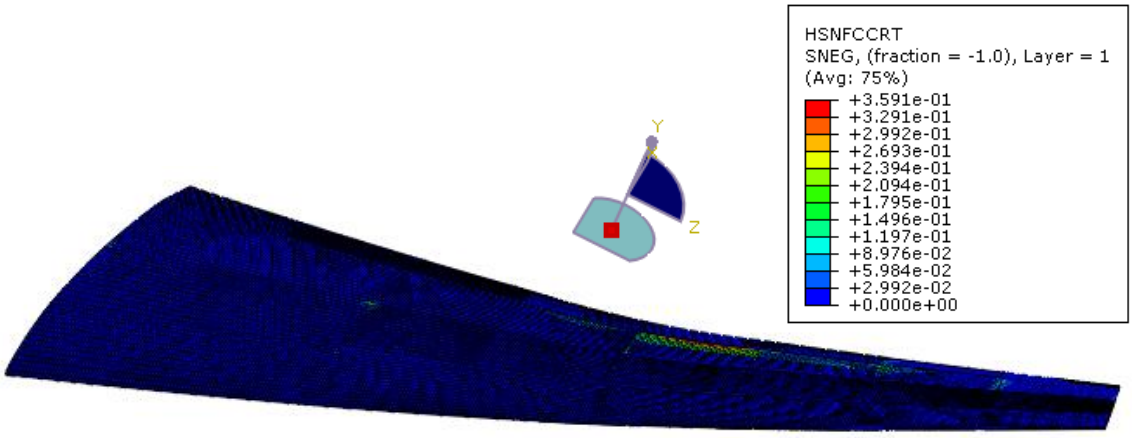

Figure 4.22 – Hashin Fiber Compression Criterion

In Figure 4.22 it can be seen that maximum stress occurs at the upper part of the wing between skin TEup3 and RSout. This is because the upper part is exposed to compression loads since the wing is bent upwards. It is happened the reverse in Figure 4.23, because the lower skin is exposed to tensile loads because of the bending moment.

In Figure 4.24, the results show that maximum stresses are at upper skin due to compressive loads, as in Figure 4.22 because of the same reason.

In Figure 4.25 happens the same as Figure 4.23, since the lower part suffers tensile loads. This last one is the more restrictive, so the wing must be optimized through matrix tension.

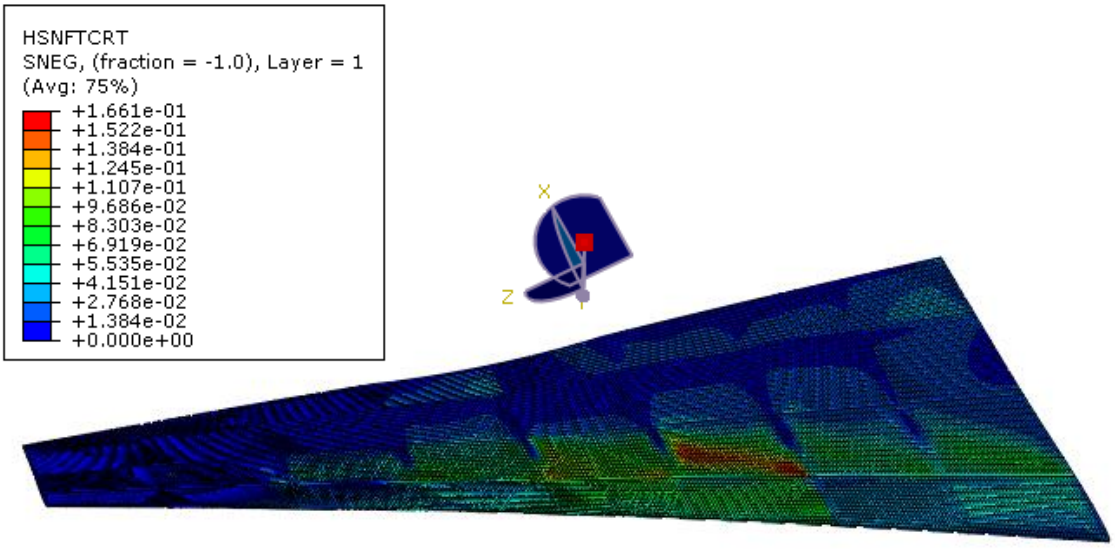

Figure 4.23 - Hashin Fiber Tension Criterion

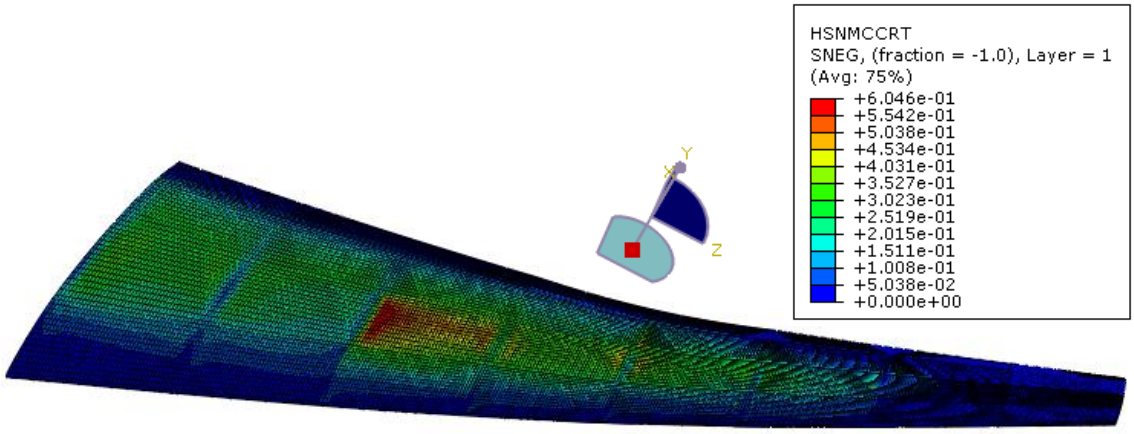

Figure 4.24 – Hashin Matrix Compression Criterion

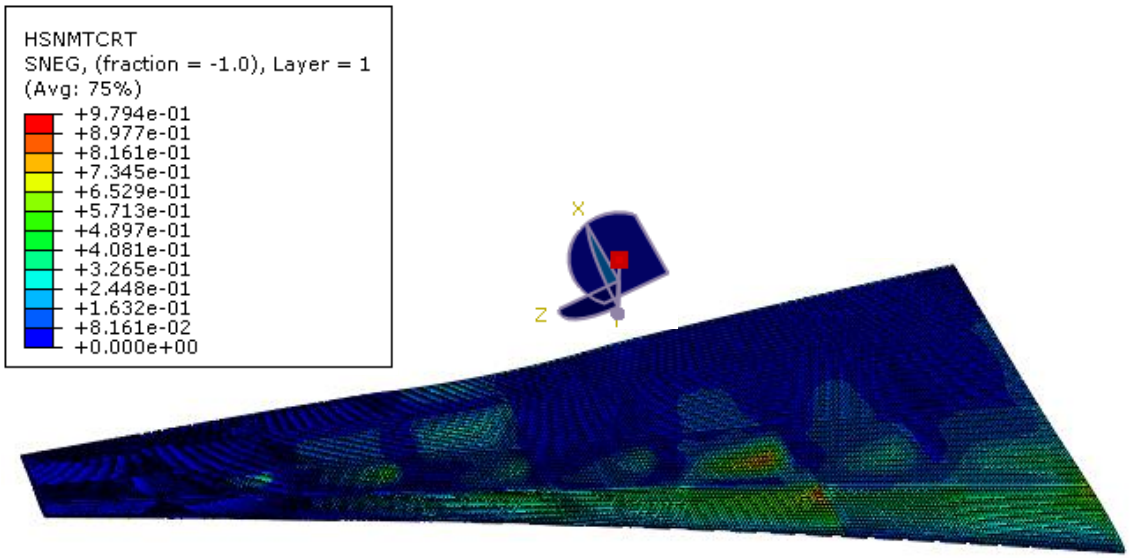

Figure 4.25 - Hashin Matrix Tension Criterion

And the result of the displacements is:

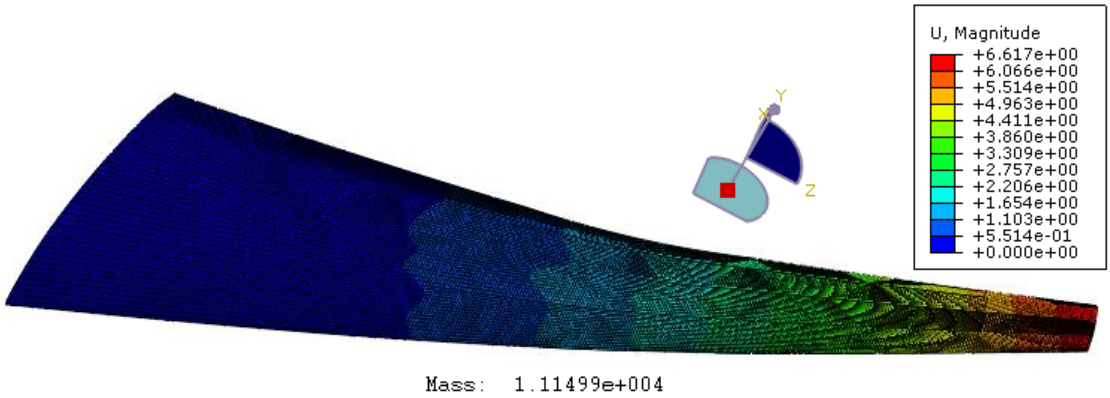

Figure 4.26 – Displacements using Carbon Matrix MTM45

HSNFCCRT	HSNFTCRT	HSNMCCRT	HSNMTCRT	$U_{max}(m)$	$M_{min}(kg)$
0.3591	0.1661	0.6046	0.9794	6.617	11149.9

Table 4.30 – Summary of results using Carbon Epoxy MTM45-1 during Cruise phase

As it was mentioned in section 4.1.2, all Hashin results obtained must be less than one. As it can be seen in Table 4.15, HSNFCCRT, HSNFTCRT, HSNMCCRT and HSNMTCRT fulfil the conditions so that the wing structure do not fail.

The objective of the optimization is obtaining a light wing, so it can be seen that from Tables 4.11 and 4.15 for Cruise phase, it is shown that Carbon Epoxy provide the lightest wing, where the minimum weight is $M_{min} = 11150\ kg$.

Thicknesses used for Carbon Epoxy MTM45 are 0.000254 m for all laminas, then the sequence used is $[45/-45/0/0/0/90]_{nS}$, which S means symmetry and the value of n for each section. This sequence is chosen due to at 0º can support better tension and compression and that is the reason of adding more laminas at that orientation. The values of n are the following:

	LEup	LEdown	TEup	TEdown
Section 1	2	3	6	9
Section 2	2	2	6	4
Section 3	2	2	5	4
Section 4	2	2	2	3

Table 4.31 - Thicknesses using Carbon Epoxy MTM45 at Skin

	FrontSpar	RearSpar
Inside	2	6
Outside	4	3

Table 4.32 - Thicknesses using Carbon Epoxy MTM45 at Spars

The sequence used for ribs is $[45/-45]_{nS}$, it is chosen to support torsion at ribs, so the value of n for each case is:

Rib 1	Rib23	Rib 45	Rib 67	Rib 89
0	2	2	2	1

Table 4.33 - Thicknesses using Carbon Epoxy MTM45 at Ribs

It is also computed the percentage of maximum displacement of the wing. From Table 4.11 and Table 4.15, maximum displacements are taken and divided into the wing length. Then:

	Al 7075-T6	Carbon Epoxy MTM45-1
Maximum displacement (%)	0.184=18.4%	0.208=20.8%

Table 4.34 - Percentage of maximum displacement

The maximum displacement occurs when Carbon Epoxy is used, because it is a composite material whose density is lower than the isotropic material, and therefore a lighter material is obtained. As the wing is lighter, the bending moment is increased and the maximum displacements are higher.

Chapter 5

Project Planning

This project is divided into five different working phases according to the objectives highlighted in section 1.2.

The first part has consisted on researching and collecting general data from the aircraft studied. These data are main characteristics and specifications of the wing aircraft to model the wing to carry out numerical aerodynamic and structural analysis.

Following this, the second part was defined to be the numerical aerodynamic analysis using 3D Panel Method to compute pressure distribution and then using Bernoulli equation to compute pressure differences.

After that, the third part is composed of modelling the wing through Abaqus/CAE to perform Numerical Structural Analysis, introducing the values of pressure from second part, the materials, thicknesses of sections and meshing the wing

Then, in the fourth part is performed an optimization of the wing to obtain a lighter wing

Finally, the last part is related to the written report, in which it is explained the method procedures, the tools used and the results obtained.

These parts are organised in such a way that it can be carried out a project planning with the estimated hours invested on it:

Working phases	Hours
Research and Collection of Data	15
Numerical Aerodynamic Analysis	70
Numerical Structural Analysis	120
Optimization	35
Report writing	85

Table 5.1 - Project Planning

Chapter 6

Regulatory and socioeconomic framework

6.1 Regulatory framework

According to regulatory framework, there are no regulations stablished for the numerical study of wings. Only regulations are applicable if the re-design of the wing is carried out. Since the wing is studied with a computer, there is no labor risks to prevent.

The wing weight is established to be maximum based on wing area and its lift generated at a safe airspeed. These standards are set by the Federal Aviation Administration with the manufacturer, so if the wing is optimized, the weight is reduced and therefore does not reach maximum allowable weight, where the optimization respects these limits established by the FAA. This reduction of weight improves efficiency and Thrust-to-Weight ratio.

6.2 Budget

In this section, it is described all costs related to the project and divided in three sections. The first section is the personal costs that relates all engineering work hours with the cost per hour. The second section is the software costs, in which software licenses are considered. Finally, the third section shows the material costs.

PERSONAL COSTS			
	Time [h]	Cost per hour [€/h]	Final Cost [€]
Engineering working hours	325	25	8125

Table 6.1 - Budget for Personal Costs

SOFTWARE COSTS			
	Time [year]	Cost per year [€/year]	Final Cost [€]
ABAQUS License	1/3	33600	11200
XFLR5 License	1/4	-	-

Table 6.2 - Budget for Software Costs

MATERIAL COSTS					
	Time [h]	Price [€]	Lifespan [h]	Price per lifespan [€/h]	Final Cost [€]
Laptop	1570	900	35040	0.0257	40.32

Table 6.3 - Budget for Material Costs

From Table 6.1, 6.2 and 6.3 the computation of personal, software and material costs are:

$$Personal\ costs\ [€] = Time[h] * Cost\ per\ hour\ [€/h] \tag{6.1}$$

$$Software\ costs\ [€] = Time[year] * Cost\ per\ year\ [€/year] \tag{6.2}$$

$$Material\ costs\ [€] = Time\ [h] * Price\ per\ lifespan[€/h] \tag{6.3}$$

6.3 Socioeconomic impact

All aerospace industries are interested on improving aircraft characteristics in terms of efficiency to reduce costs. Optimization of the weight is one of objectives carried out by an industry to improve efficiency. This case studies how to optimize the wing weight so that an aircraft with lighter weight can have more sales when the improvements are carried out.

This study can lead to give safety to customers like airlines, in such a way that they purchase better aircraft. If Airlines purchase more aircrafts of this kind, it will provide more safety to passengers and therefore, manufacture industries and airlines increase revenues and profits.

Chapter 7

Conclusions

This project has proved that 3D Panel Method and FEM are meaningful methods for aerodynamic and structural analysis respectively, using tools as XFLR5 and Abaqus/CAE. Pressure differences obtained at the surface of the wing from 3D Panel Method, simulate real aerodynamic loads around the wing for all flight phases. Applying BC and introducing these values, the wing works as a real model, since finally compute maximum stresses and maximum vertical displacements.

- Assymetric airfoils produce higher lift at a lower AoA to avoid stall
- 3D Panel Method shows a more detail C_p distribution around the wing than other numerical aerodynamic methods, so pressure difference results are more accurate.
- Dynamic pressure is higher during cruise phase since it proportionally depends on the square Mach number.
- The higher minimum weight is obtained at cruise conditions due to pressure difference are higher at cruise phase and therefore wing sections must have more thickness.
- The use of composite materials is better than isotropic materials, because it provides a lighter wing.
- Composite material ply orientation is important to optimize the wing weight.
- A drawback of using composite materials is that results in a higher maximum displacement than isotropic materials. The solution is reducing maximum swept angle, in such a way that the percentage of displacement do not exceed twenty percent.
- The criteria ply orientation is chosen depending on the displacement conditions. Since maximum displacement occurs in vertical axis, at the upper surface is acting compression loads and at the lower surface is acting tension loads, both in longitudinal direction, so more laminas are located in this direction (0 degrees), but it is necessary use laminas in transverse direction and 45/-45 degrees orientation to avoid failure.
- Ribs are orientated at [45/-45] to avoid failure due to torsion.

BIBLIOGRAPHY

[1] "The aviation history online" http://www.aviation-history.com/theory/airfoil.htm Consultation year: 2017

[2] "A brief history of aircraft structures" http://aerospaceengineeringblog.com/aircraft-structures/ Consultation year: 2017

[3] "Aircraft performing all flight phases" http://www.lufthansa.com Consultation year: 2017

[4] "Take-off and Landing" Lecture 1.5 from Flight Mechanics Notes Course 2015/2016

[5] "Air charter service A340 600"http://www.aircharterservice.es/guia-de-avions/charter-en-grupos/airbus- europe/airbusa340-600 Consultation year: 2017

[6] "Modern airliners" http://www.modernairliners.com/airbus-a340-specs/ Consultation year: 2017

[7] "Aircraft characteristics airport and maintenance planning" http://www.aircraft.airbus.com/fileadmin/media_gallery/files/tech_data/AC/Airbus-AC_A340-500_600-Dec16.pdf Consultation year: 2017

[8] "Apollo Canard – XFLR5" http://www.apollocanard.com/6_xflr5.htm Consultation year: 2017

[9] "Introduction to finite element analysis (general steps)" Introduction to Structural Analysis Notes. Bachelor in Aerospace Engineering

[10] "Abaqus/CAE User's Guide" Dassault Systems http://abaqus.software.polimi.it/v6.14/pdf_books/CAE.pdf Consultation year: 2017

[11] "Getting started with Abaqus: Interactive Edition" http://abaqus.software.polimi.it/v6.14/books/gsa/default.htm?startat=ch02.html

[12] "Airfoil Tools" http://airfoiltools.com Consultation year: 2017

[13] "High Lift Devices" Aerodynamics Notes. Bachelor in Aerospace Engineering

[14] "Generalities and Operating Environment" Chapter 1 from Aircraft Design Notes. Bachelor in Aerospace Engineering

[15] "Skybrary Airbus A-340-600" https://www.skybrary.aero/index.php/A346 Consultation year: 2017

[16] "ASM Aerospace Specification Metals Inc" http://asm.matweb.com/search/SpecificMaterial.asp?bassnum=MA7075T6

[17] "Analysis of a wing structure by Finite Element Software" Aerospace Structures. Bachelor in Aerospace Engineering

[18] "Aircraft Structures for Engineering Students" Fourth Edition. T.H.G Megson